

# Spot the difference

## Impact of different selection criteria on observed properties of passive galaxies in zCOSMOS-20k\* sample

M. Moresco<sup>1</sup>, L. Pozzetti<sup>2</sup>, A. Cimatti<sup>1</sup>, G. Zamorani<sup>2</sup>, M. Bolzonella<sup>2</sup>, F. Lamareille<sup>3</sup>, M. Mignoli<sup>2</sup>, E. Zucca<sup>2</sup>, S.J. Lilly<sup>4</sup>, C.M. Carollo<sup>4</sup>, T. Contini<sup>3,5</sup>, J.-P. Kneib<sup>6</sup>, O. Le Fèvre<sup>6</sup>, V. Mainieri<sup>7</sup>, A. Renzini<sup>8</sup>, M. Scodreggio<sup>9</sup>, S. Bardelli<sup>2</sup>, A. Bongiorno<sup>10</sup>, K. Caputi<sup>2,3</sup>, O. Cucciati<sup>2</sup>, S. de la Torre<sup>11</sup>, L. de Ravel<sup>11</sup>, P. Franzetti<sup>9</sup>, B. Garilli<sup>9</sup>, A. Iovino<sup>12</sup>, P. Kampczyk<sup>4</sup>, C. Knobel<sup>4</sup>, K. Kovač<sup>4</sup>, J.-F. Le Borgne<sup>3,5</sup>, V. Le Brun<sup>6</sup>, C. Maier<sup>4,24</sup>, R. Pello<sup>3,5</sup>, Y. Peng<sup>13</sup>, E. Perez-Montero<sup>3,5</sup>, V. Presotto<sup>12</sup>, J.D. Silverman<sup>14</sup>, M. Tanaka<sup>14</sup>, L. Tasca<sup>6</sup>, L. Tresse<sup>6</sup>, D. Vergani<sup>15</sup>, L. Barnes<sup>4</sup>, R. Bordoloi<sup>4</sup>, A. Cappi<sup>2</sup>, C. Diener<sup>4</sup>, A.M. Koekemoer<sup>13</sup>, E. Le Floch<sup>16</sup>, C. López-Sanjuan<sup>6,22</sup>, H.J. McCracken<sup>17</sup>, P. Nair<sup>2,13</sup>, P. Oesch<sup>4,18</sup>, C. Scarlata<sup>19</sup>, N. Scoville<sup>20</sup>, and N. Welikala<sup>21</sup>

(Affiliations can be found after the references)

Received – – –; accepted – – –

### ABSTRACT

*Aims.* We present the analysis of photometric, spectroscopic, and morphological properties for differently selected samples of passive galaxies up to  $z = 1$  extracted from the zCOSMOS-20k spectroscopic survey. This analysis intends to explore the dependence of galaxy properties on the selection criterion adopted, study the degree of contamination due to star-forming outliers, and provide a comparison between different commonly used selection criteria. This work is a first step to fully investigating the selection effects of passive galaxies for future massive surveys such as Euclid.

*Methods.* We extracted from the zCOSMOS-20k catalog six different samples of passive galaxies, based on morphology (3336 “morphological” early-type galaxies), optical colors (4889 “red-sequence” galaxies and 4882 “red UVJ” galaxies), specific star-formation rate (2937 “quiescent” galaxies), a best fit to the observed spectral energy distribution (2603 “red SED” galaxies), and a criterion that combines morphological, spectroscopic, and photometric information (1530 “red & passive early-type galaxies”). For all the samples, we studied optical and infrared colors, morphological properties, specific star-formation rates, and the equivalent widths of the residual emission lines; this analysis was performed as a function of redshift and stellar mass to inspect further possible dependencies.

*Results.* We find that each passive galaxy sample displays a certain level of contamination due to blue/star-forming/nonpassive outliers. The morphological sample is the one that presents the higher percentage of contamination, with  $\sim 12$ -65% (depending on the mass range) of galaxies not located in the red sequence,  $\sim 25$ -80% of galaxies with a specific star-formation rate up to  $\sim 25$  times higher than the adopted definition of passive, and significant emission lines found in the median stacked spectra, at least for  $\log(\mathcal{M}/M_{\odot}) < 10.25$ . The red & passive ETGs sample is the purest, with a percentage of contamination in color  $< 10\%$  for stellar masses  $\log(\mathcal{M}/M_{\odot}) > 10.25$ , very limited tails in sSFR, a median value  $\sim 20\%$  higher than the chosen passive cut, and equivalent widths of emission lines mostly compatible with no star-formation activity. However, it is also the less economic criterion in terms of information used. Among the other criteria, we found that the best performing are the red SED and the quiescent ones, providing a percentage of contamination only slightly higher than the red & passive ETGs criterion (on average of a factor of  $\sim 2$ ) but with absolute values of the properties of contaminants still compatible with a red, passively evolving population. We also find a strong dependence of the contamination on the stellar mass and conclude that, almost irrespective of the adopted selection criteria, a cut at  $\log(\mathcal{M}/M_{\odot}) > 10.75$  provides a significantly purer sample in terms of star-forming contaminants. By studying the restframe color-mass and color-color diagrams, we provided two revised definitions of passive galaxies based on these criteria that better reproduce the observed bimodality in the properties of zCOSMOS-20k galaxies.

The analysis of the number densities of the various samples shows evidences of mass-assembly “downsizing”, with galaxies at  $10.25 < \log(\mathcal{M}/M_{\odot}) < 10.75$  increasing their number by a factor  $\sim 2$ -4 from  $z = 0.6$  to  $z = 0.2$ , by a factor  $\sim 2$ -3 from  $z = 1$  to  $z = 0.2$  at  $10.75 < \log(\mathcal{M}/M_{\odot}) < 11$ , and by only  $\sim 10$ -50% from  $z = 1$  to  $z = 0.2$  at  $11 < \log(\mathcal{M}/M_{\odot}) < 11.5$ .

**Key words.** galaxies: evolution – galaxies: fundamental parameters – galaxies: statistics – surveys

### 1. Introduction

Early-type galaxies (ETGs) represent a population of galaxies apparently simple and homogeneous in terms of morphology, colors, stellar population content, and scaling relations (for a detailed review, see Renzini, 2006, and references therein), at least in the local Universe. Originally

Send offprint requests to: Michele Moresco (e-mail: michele.moresco@unibo.it)

\* based on data obtained with the European Southern Observatory Very Large Telescope, Paranal, Chile, program 175.A-0839

(Hubble, 1936), this population of galaxies was identified just on the basis of its morphology, with early-type galaxies having a rounder, elliptical shape and late-type galaxies being characterised by spiral features. Very soon, however, it was evident that this morphological dichotomy also reflected a difference in terms of the stellar population content and that the two classifications (morphological and based on the stellar population content) correlate, even if they were far from overlapping.

It has been evident for almost 50 years now that galaxy rest-frame colors show a clear bimodal distribution, both in clusters (e.g., Visvanathan & Sandage, 1977; Tully et al., 1982) and in the field (Strateva et al., 2001; Hogg et al., 2002; Baldry et al., 2004a,b; Bell et al., 2004; Franzetti et al., 2007). Later studies have also shown a bimodality in many other galaxy parameters:  $H\alpha$  (Balogh et al., 2004) and [OII] (Mignoli et al., 2009) emission, 4000 Å break (Kauffmann et al., 2003), star-formation history (Brinchmann et al., 2004), and clustering (Meneux et al., 2006). A similar bimodality has also been found in the galaxy stellar mass function, showing that early-type galaxies are the most massive galaxies at  $z \sim 0$  (Baldry et al., 2004a, 2006, 2008) and dominate the massive end of the stellar mass function up to  $z \sim 1$  (Pozzetti et al., 2010).

The properties of ETGs make them the ideal candidates to also probe cosmology, together with galaxy formation models and theories. These galaxies have been found to have a stronger clustering with respect to late-type galaxies (e.g., see Zehavi et al., 2011, and references therein), providing a better tracer to the structure of underlying matter. It has also been proposed to use this population of galaxies as “cosmic chronometers”, able to trace the differential age evolution of the Universe as a function of redshift (Jimenez et al., 2002) and provide independent and precise measurements of the Hubble parameter  $H(z)$  up to  $z \sim 1.5$  (Simon et al., 2005; Stern et al., 2010; Moresco et al., 2012a). These measurements have been demonstrated to be an innovative and complementary tool to constrain cosmological parameters (Moresco et al., 2011, 2012b; Wang et al., 2012; Riemer-Sørensen et al., 2013; Aviles et al., 2013; Said et al., 2013).

A powerful tool to study the evolution of a galaxy population is analyzing the evolution of its number density as a function of redshift, because this can give hints of the processes and characteristic timescales involved. The number density of ETGs has been deeply studied by many authors, and there is a general agreement that, while there is a strong evolution for less massive galaxies, the number density of  $\log(M/M_{\odot}) > 11$  ETGs is almost unchanged from  $z \sim 1$  to  $z \sim 0$  (Cimatti et al., 2006; Scarlata et al., 2007; Pozzetti et al., 2010; Brammer et al., 2011; Maraston et al., 2012; Ilbert et al., 2013; Moustakas et al., 2013). This has been interpreted as evidence that this population of galaxy has been already in place since  $z \sim 1$ .

These pieces of observational evidence have induced a gradual shift of notation, so that with time the definition of “early-type” has been not only related to a morphological feature but also to peculiar properties in terms of the stellar population content. The ETGs are now usually identified as spheroidal (E/S0) galaxies with old stellar population, no (or negligible) star formation, and a passive evolution as a function of cosmic time. Recently, all these proper-

ties are often used without a clear distinction, and “red”, “quiescent”, and “old” are erroneously used as synonyms. Surely, as discussed above, the bimodality in many galaxy properties highlights that red galaxies are mostly quiescent and passively evolving; however, a detailed and quantitative estimate of the contamination due to blue/star-forming outliers should be made before doing a one-to-one correspondence. Franzetti et al. (2007) pointed out such possible contamination when studying a color-selected sample of ETGs, concluding that selecting galaxies only on the basis of their colors can be misleading in estimating the evolution of old and passively evolving galaxies.

In this paper, we want to thoroughly explore what kind of galaxies are culled by different selection criteria, either purely morphological or based on the stellar population content as characterized by colors or star-formation rate (SFR). In particular, we shall quantify to which extent these criteria overlap in terms of selected galaxies and to which extent they differ. Various global properties of the different samples are presented and discussed. In Sect. 2 we present our data and how the different samples of passive galaxies have been selected. In Sect. 3 the color, spectroscopic, and morphological analysis are presented. In Sect. 4 we quantify how much each sample is contaminated by the presence of blue/star-forming outliers and how this contamination depends on the stellar mass and on the adopted selection criterion. We also analyze the number densities of the various samples and compare them to check for differences and provide insights about the characteristic processes involved. Finally, we also present two revised color-mass and color-color selection criteria of passive galaxies, aiming to reduce the contamination by blue star-forming galaxies.

This study is interesting in the view of many upcoming surveys (e.g., Euclid, Laureijs et al., 2011) since it provides a comparison between different methods of selecting passive galaxies, quantifying the purity of the sample as well as the cost in terms of information needed.

Throughout the paper, we adopt the cosmological parameters  $H_0 = 70 \text{ km s}^{-1} \text{ Mpc}^{-1}$ ,  $\Omega_m = 0.25$ ,  $\Omega_{\Lambda} = 0.75$ . Magnitudes are quoted in the AB system.

## 2. Data

### 2.1. The sample

The COSMOS Survey (Scoville et al., 2007) has imaged a field of  $\sim 2 \text{ deg}^2$  with the Advanced Camera for Surveys (ACS) with single-orbit I-band exposures to a depth  $I_{AB} \simeq 28 \text{ mag}$  and 50% completeness at  $I_{AB} = 26.0 \text{ mag}$  for sources  $0.5''$  in diameter (Koekemoer et al., 2007).

The analysis presented in this paper is based on the zCOSMOS spectroscopic survey (Lilly et al., 2007, 2009). This ESO Large Programme ( $\sim 600$  hours of observations) was aiming to map the COSMOS field with the Visible Multi-Object Spectrograph (VIMOS, Le Fèvre et al., 2003), mounted on the ESO Very Large Telescope (VLT). Our sample has been extracted from the zCOSMOS 20k bright sample (Lilly et al., 2009). The observed magnitudes in 12 photometric bands (CFHT  $u^*$ ,  $K$  and  $H$ , Subaru  $B_J$ ,  $V_J$ ,  $g^+$ ,  $r^+$ ,  $i^+$ , and  $z^+$ , UKIRT  $J$  and Spitzer IRAC at  $3.6 \mu\text{m}$  and  $4.5 \mu\text{m}$ ) have been used in order to derive reliable estimates of galaxy parameters from the photometric SED fitting. The photometric

catalog is described in Capak et al. (2007). Following their approach, magnitudes were corrected for Galactic extinction using Table 11 of Capak et al. (2007), and the photometry was optimized by applying zeropoint offsets to the observed magnitudes to reduce differences between the observed and reference magnitudes computed from a set of template spectral energy distributions (SEDs). The spectra have a medium resolution grism ( $R \approx 600$ ) with a slit width of 1 arcsec; the spectral ranges of the observations are typically 5550 – 9650 Å. The data were reduced with VIMOS Interactive Pipeline Graphical Interface software (VIPGI, Scodreggio et al., 2005) and the redshift measured with EZ software (Garilli et al., 2010) with a high success rate ( $\approx 95\%$  in the redshift range  $0.5 < z < 0.8$ , Lilly et al., 2009). The line measurements were performed using the program *Platefit* (see Lamareille et al., 2006, for further details). After removing the spectroscopically confirmed stars, the broad-line AGNs, and the galaxies with an insecure redshift measurement ( $z_{\text{flag}} < 1.5$ ), we end up with a parent sample of 17211 galaxies.

The stellar masses ( $\mathcal{M}$ ) and SFRs were estimated for the entire sample by performing a best fit to the SEDs, using the observed magnitudes in 12 photometric bands from  $u^*$  to  $4.5\mu\text{m}$ . A grid of theoretical models was built from Bruzual & Charlot (2003) stellar population synthesis models (hereafter BC03), adopting an exponentially declining star-formation history (SFH) with  $\tau = 0.1, 0.3, 0.6, 1, 2, 3, 5, 10, 15, 30$  Gyr, a Chabrier initial mass function (Chabrier, 2003), a solar stellar metallicity, and a Calzetti extinction law (Calzetti et al., 2000) with  $0 < A_V < 3$ . Absolute magnitudes and colors were evaluated using the “algorithm for luminosity function” (ALF) software following the method described in Zucca et al. (2009). The specific Star Formation Rate (sSFR) has been defined as the ratio between the SFR and the stellar mass,  $\text{sSFR} = \text{SFR}/\mathcal{M}$ .

## 2.2. The selection criteria

Different selection criteria have been proposed so far to select passive galaxies. We exploit here six different definitions, which are described below. These criteria were chosen so as not to be too restrictive because otherwise we would have poor completeness, but at the same time to minimize the contamination by blue, star-forming objects.

- **“morphological” ETGs.** The Zürich Estimator of Structural Types (ZEST; Scarlata et al., 2007) estimates the morphological type of galaxies with a combination of a principal component analysis (PCA) of five nonparametric diagnostics of galaxy structure (asymmetry, concentration, Gini coefficient, second-order moment of the brightest 20% galaxy pixels, and ellipticity) and of a parametric description of the galaxy light (the exponent of a single-Sérsic fit to the surface brightness distribution). This estimator was applied to the full zCOSMOS-20k sample, providing morphological measurements for all the galaxies. We refer to Scarlata et al. (2007) for a discussion concerning the classification uncertainties using this method. Following this classification, we selected 3336 ETGs matching an E/S0 morphology (Scarlata et al., 2007).
- **“red-sequence” galaxies.** In their analysis, Peng et al. (2010) defined a color-mass relation

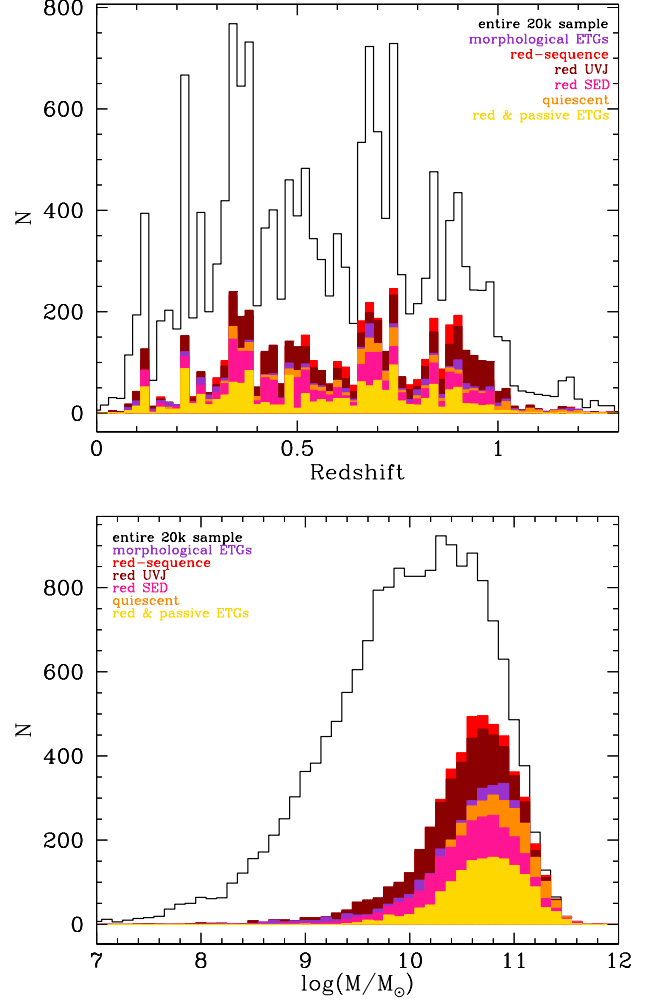


**Fig. 1.** Redshift distribution (upper panel) and stellar mass distribution (lower panel) of the entire zCOSMOS-20k sample and of the different sample. In violet the morphological ETGs, in light red the red-sequence galaxies, in dark red the red UVJ galaxies, in pink the red SED galaxies, in orange the quiescent galaxies, and in yellow the red & passive ETGs.

calibrated on Sloan Digital Sky Survey (SDSS) and zCOSMOS-10k data, dividing red-sequence from blue-cloud galaxies. This relation also takes the redshift evolution into account and is a weak function of mass. Following their approach, 4889 red galaxies were selected on the basis of the following dividing rest-frame ( $U - B$ ) color.

$$(U - B)_{\text{rest}} > 1.10 + 0.075 \times \log\left(\frac{\mathcal{M}}{10^{10} \mathcal{M}_{\odot}}\right) - 0.18 \times z$$

- **“red UVJ” galaxies.** Following Williams et al. (2009), we extracted a sample of galaxies on the basis of the restframe color-color diagram defined as

$$(U - V)_{\text{rest}} > 0.88 \times (V - J)_{\text{rest}} + 0.69 \quad [0 < z < 0.5]$$

$$(U - V)_{\text{rest}} > 0.88 \times (V - J)_{\text{rest}} + 0.59 \quad [0.5 < z < 1],$$

	morphology	red sequence	red UVJ	red SED	quiescent	red & passive ETGs	% w.r.t. global sample
morphology	<b>3336</b>	77.0%	76.9%	48.6%	56.4%	33.0%	19.4%
red sequence	52.5%	<b>4889</b>	83.2%	51.4%	59.3%	31.0%	28.4%
red UVJ	52.6%	83.3%	<b>4882</b>	49.9%	57.6%	30.7%	28.4%
red SED	62.3%	96.6%	93.5%	<b>2603</b>	84.7%	46.3%	15.1%
quiescent	64.0%	98.7%	95.8%	75.1%	<b>2937</b>	47.0%	17.1%
red & passive ETGs	72.0%	99.2%	98.0%	78.8%	90.2%	<b>1530</b>	8.9%

**Table 1.** Passive galaxy samples overlap depending on the different selection criteria adopted and number of galaxies (in boldface). Each box gives the percentage of galaxies of a particular sample (specified by the row’s name) found in another sample (specified by the column’s name). The last column also reports the percentage number of each sample with respect to the parent zCOSMOS-20k sample of 17211 galaxies.

with the additional constraints of  $(U - V)_{\text{rest}} > 1.3$  and  $(V - J)_{\text{rest}} < 1.6$ . With these cuts, we selected 4882 galaxies.

- **“red SED” galaxies.** Ilbert et al. (2009) employed a set of templates, generated by Polletta et al. (2007) with the code GRASIL (Silva et al., 1998), to fit the VIMOS VLT Deep Survey (VVDS) sources (Le Fèvre et al., 2005) from the UV-optical to the mid-IR. Therefore, this set of templates provides a better joining of UV and mid-IR than those previously proposed by (Ilbert et al., 2006). The nine galaxy templates of Polletta et al. (2007) include three SEDs of elliptical galaxies and six templates of spiral galaxies (S0, Sa, Sb, Sc, Sd, Sdm). Twelve additional templates obtained from BC03 models with starburst ages ranging from 3 to 0.03 Gyr are also added to better represent the data. Finally, the templates were linearly interpolated, so that a total set of 32 templates was obtained. These templates were used to estimate photometric types from a best fit to the observed photometry without additional dust extinction. With this method, we selected 2603 galaxies best fitted with an early-type template (i.e., SED-type from 1 to 8).
- **“quiescent” galaxies.** Following Ilbert et al. (2010) and Pozzetti et al. (2010), we selected 2937 quiescent galaxies on the basis of their sSFR, adopting the cut  $\log(\text{sSFR}) < -2$  [ $\text{Gyr}^{-1}$ ]. As shown by Ilbert et al. (2010), this cut corresponds almost directly to a cut  $(\text{NUV} - r_+)_{\text{template}} > 3.5$ , with which they defined their sample of quiescent galaxies. With these selection criteria, we select galaxies that are increasing their mass at a rate less than 1/100th of their present mass.
- **“red & passive ETGs”.** To obtain a reliable sample with as little bias as possible due to the presence of star-forming contaminants, we decided to follow the approach used in Moresco et al. (2010). From the parent sample, 1530 ETGs were extracted by combining photometric, morphological, and optical spectroscopic criteria: galaxies were chosen with a best fit to the SED matching a local E-S0 template (using the CWW templates of Ilbert et al., 2006), weak/no emission lines ( $\text{EW}_0([\text{OII}]/\text{H}\alpha) < 5$  Å), spheroidal morphology, and an observed  $(K - 24\mu\text{m})$  color typical of E/S0 local galaxies (i.e.,  $(K - 24\mu\text{m}) < -0.5$ ); for further details about the sample selection, see Moresco et al. (2010).

Other standard definitions involve, for example, different sets of templates to perform a best-fit match to the observed SED (CWW photometric types, Ilbert et al.,

2006) or different cuts in the observed colors, as for the case of luminous red galaxies (LRG, Eisenstein et al., 2001) and Baryon Oscillation Spectroscopic Survey (BOSS, Schlegel et al., 2009) samples. We checked, however, that the performances of these criteria are much worse than those of the other samples selected in our analysis in the selection of a pure sample of passive galaxies. In particular, LRGs and BOSS selections were optimized for the specific properties of those surveys and cannot straightforwardly be applied to zCOSMOS survey; we refer to Masters et al. (2011) for a discussion of the contamination by late-type morphological types of BOSS galaxies.

In Fig. 1 we show the redshift and mass distribution of the various samples. Each sample was further divided into six subsamples after we considered separately two redshift ranges ( $z \leq 0.5$  and  $z > 0.5$ ), three mass ranges (low-mass  $\log(\mathcal{M}/\mathcal{M}_\odot) < 10.25$ , medium-mass  $10.25 \leq \log(\mathcal{M}/\mathcal{M}_\odot) < 10.75$ , and high-mass  $\log(\mathcal{M}/\mathcal{M}_\odot) \geq 10.75$ ) in order to be able to discern the dependencies on mass and redshift.

In Tab. 1 we report the number of galaxies obtained with the different selections, as well as the percentage overlap between the various samples. As expected, the overlap between samples obtained with different selection criteria is often partial, suggesting that they have different properties. In particular, we notice that there is a small overlap between all samples and the morphologically selected sample, indicating that a large fraction of passive galaxies selected on the basis of colors, or more generically on the basis of photometric properties, do not have an E/S0 morphology (see Sect. 3.3). The overlap is also small when considering how many morphologically selected ETGs are found in the other samples, indicating that a non negligible fraction of ellipticals have blue colors. The overlap is, instead, larger when considering the other samples. The red-sequence and red UVJ samples provide an almost identical number of galaxies and show a similar reciprocal overlap of  $\sim 80\%$ . However, as we see in the following section, they have different photometric properties. The fraction of galaxies overlapping with the red-sequence sample is above  $\sim 80\%$ , irrespective of the selection criterion considered; however this is probably due to the higher number of galaxies of that sample. What is more interesting is to consider the fraction of galaxies included in the quiescent sample: the overlap with the red SED and the red & passive ETGs samples is above  $\sim 85\%$ , which testifies a quiescent star-formation activity. However, for the red-sequence and the red UVJ samples, the overlap is  $\sim 60\%$ , indicating that almost half of that sample have a higher star-formation activity. The last

remark is about the red & passive ETGs criterion, which presents a small overlap with all the other samples: this is partly because of the smaller number of galaxies included in this sample and partly because this is the only sample also comprising a spectroscopic cut (see Sect. 3.2).

### 3. The analysis

As already discussed, the ETGs population is rather homogeneous in color, star-formation activity, and morphology. We therefore decided to inspect in detail different properties to study how their global properties change for the different samples.

#### 3.1. Color properties

The primary observable, apart from the morphology, that we decided to examine, is the color. We decided to study both the standard  $(U - B)_{\text{rest}}$  color-mass and  $(U - V)_{\text{rest}}$ - $(V - J)_{\text{rest}}$  color-color plots, as well as an IRAC color-color diagram as first introduced by Lacy et al. (2004).

The  $(U - B)_{\text{rest}}$ -mass diagram is shown for both redshift ranges ( $z \leq 0.5$  and  $z > 0.5$ ) in Fig. 2. The gray hatched area represents the region that falls outside what is considered the red sequence, as defined by Peng et al. (2010) and previously reported. The clearest evidence is that most samples lie as expected in the red-sequence region; this is not surprising, since most selection criteria are based (or partially based) on an optical-color selection. For the morphologically selected ETGs, we found a confirmation of what was deduced from Tab. 1, i.e., that this sample is contaminated by the presence of a non-negligible tail of galaxies with blue  $(U - B)_{\text{rest}}$  colors ( $\sim 12$ -65%), both at high and low redshifts. Quite surprising is the tail of red UVJ galaxies with blue color, which even forms a second peak in the  $(U - B)_{\text{rest}}$  distribution at  $z \leq 0.5$  (as shown in Fig. 2). This tail is due to the fact that the cut proposed by Williams et al. (2009) does not perfectly fit the observed bimodality in the UVJ diagram of the zCOSMOS-20k sample.

The  $(U - V)_{\text{rest}}$ - $(V - J)_{\text{rest}}$  diagram provides complementary information with respect to the color-mass diagram. As in the previous plot, we notice that the red & passive ETGs, the quiescent galaxies, and the red SED samples well fit the passive region defined by Williams et al. (2009) and identified by the non-hatched region of Fig. 3; we also observe as before the quite prominent tail of morphological ETGs with quite blue colors. Less expected is the fact that the red-sequence galaxies display a non-negligible fraction of galaxies which do not fit perfectly the passive UVJ region. We will further discuss the issue of the different behavior of red-sequence and red UVJ galaxies in Sect. 4.5.

The IRAC observed color-color plot is more interesting since these colors less directly (or not at all) influence the various selection criteria and are therefore a better indication of how much the samples are biased. As defined by Lacy et al. (2004), we plotted the  $8.0 \mu\text{m}/4.5 \mu\text{m}$  ratio against the  $5.8 \mu\text{m}/3.6 \mu\text{m}$  ratio in Fig. 4. This plot was initially introduced to identify active galactic nuclei (AGN) candidates, which should lie in the region identified by the dotted lines. More recently, Donley et al. (2012) revised this selection criterion to reduce the contamination by normal star-forming galaxies by narrowing the re-

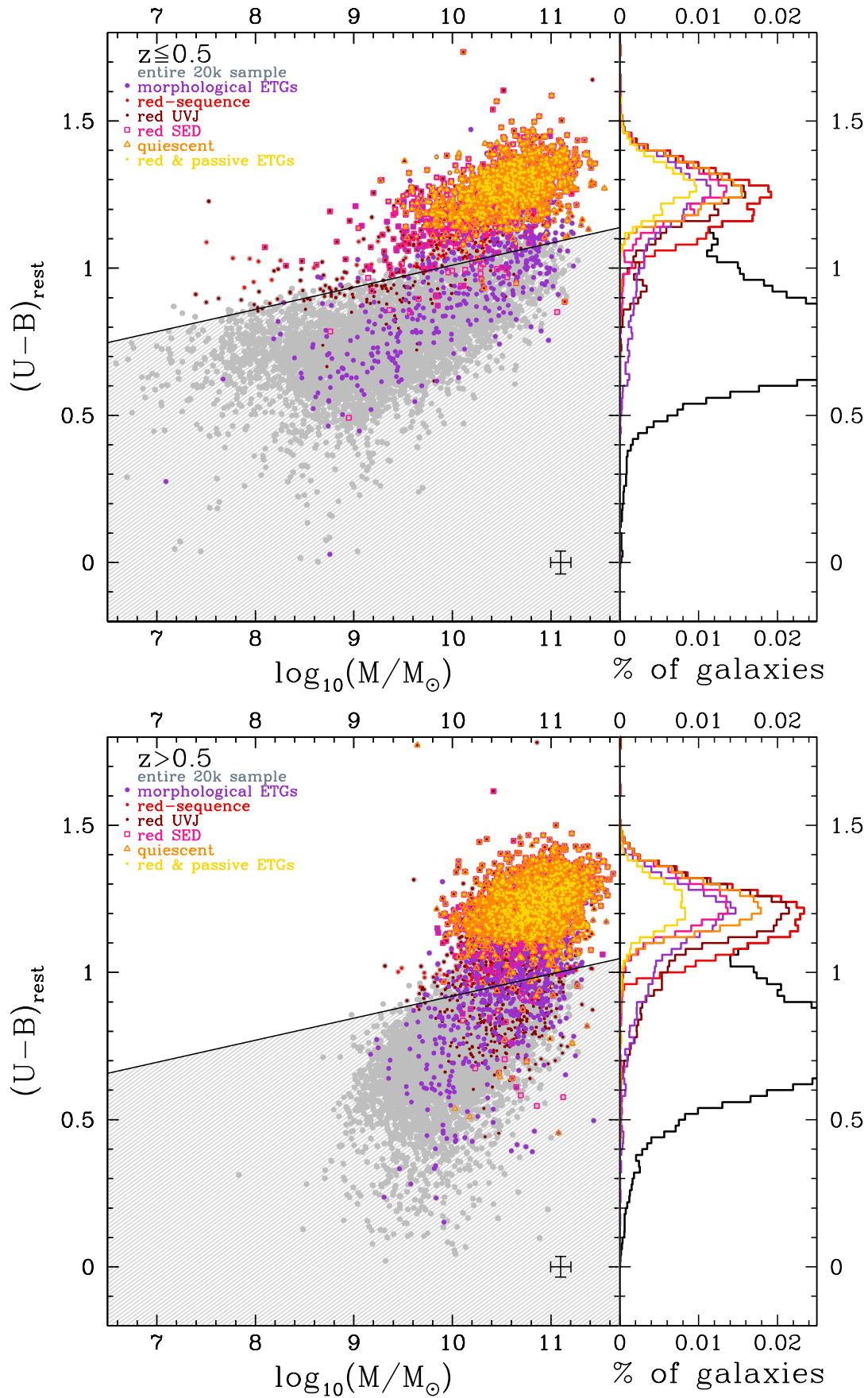
gion where the AGN candidates should lie (the area identified by the dashed lines). In their work, they also studied the predicted  $z = 0 - 3$  IRAC colors of different templates as a function of the AGN fraction, considering a star-forming template, a starburst, a normal star-forming spiral galaxy, and an elliptical galaxy. By analyzing the tracks of the elliptical galaxies, we found that they occupy a very specific region of the IRAC color-color diagram, i.e.,  $\log(S_{8.0}/S_{4.5}) < -0.1 \cap \log(S_{5.8}/S_{3.6}) < -0.1$ , at least up to  $z \sim 2$ ; this region is indicated as the non-hatched region of Fig. 4. From this plot, it is evident that in both redshift ranges most of the samples are well located in a clump inside the region just defined; however, different from the color diagrams, there are more pronounced tails outside this region. At  $z \leq 0.5$  almost all samples show a very significant vertical tail with blue colors in  $S_{5.8}/S_{3.6}$  and red colors in  $S_{8.0}/S_{4.5}$ , which is a region in which low-redshift star-forming galaxies lie (for a comparison, see Fig. 2 of Donley et al., 2012). In contrast, for  $z > 0.5$  the tails move toward red colors in both  $S_{5.8}/S_{3.6}$  and  $S_{8.0}/S_{4.5}$ . Even if they fall inside the AGN candidate region defined by Lacy et al. (2004), it is very likely that most of these galaxies are higher redshift star-forming galaxies, as can be found following the tracks of Donley et al. (2012).

#### 3.2. Spectroscopic properties

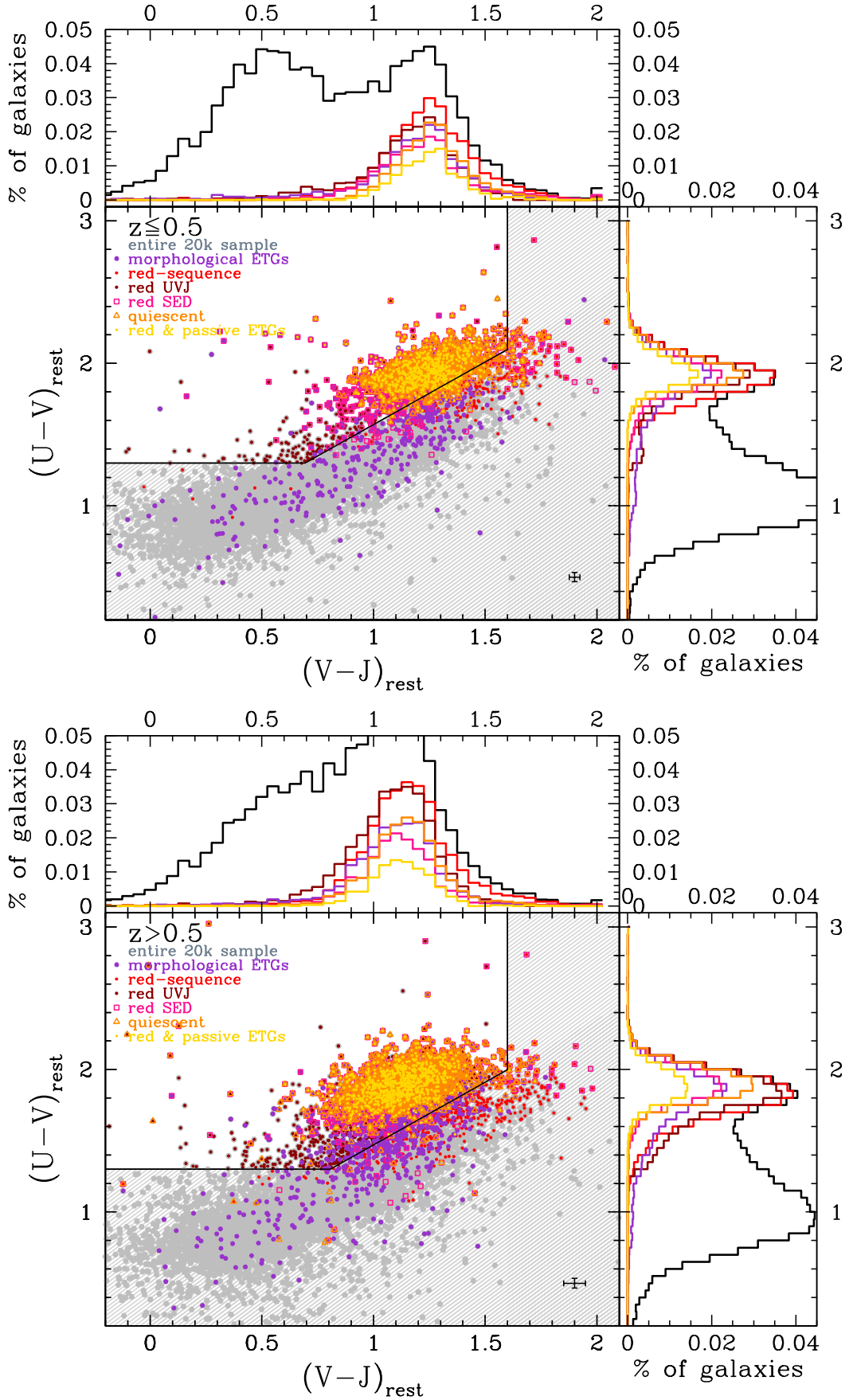
The spectroscopic properties of the galaxies have not been used (except in the red & passive ETGs criterion) to select passive galaxies; therefore, they may provide interesting insights concerning the contamination of the various samples. We decided to look at the restframe equivalent widths ( $EW_0$ ) of [OII] and H $\alpha$  lines since they are well-known indicators of star-formation activity. Given the wavelength coverage of zCOSMOS spectra, the two lines are not present in both redshift ranges: in particular H $\alpha$  line is observable at  $z \leq 0.5$ , while [OII] is observable at  $z > 0.5$ . These lines will be compared with another indicator of star formation, the sSFR, which provides the relative contribution of the SFR by weighting it with the total stellar mass of the galaxy.

Figure 5 shows  $\log(\text{sSFR}/\text{Gyr}^{-1})$  versus  $EW_0(\text{H}\alpha)$  (upper panel;  $z > 0.5$ ) and  $EW_0([\text{OII}])$  (lower panel;  $z \leq 0.5$ ). As expected, there exists a correlation (even if with a large dispersion) between the sSFR and the equivalent widths of [OII] and H $\alpha$  emission lines. Ilbert et al. (2010), aiming to study the galaxy stellar mass assembly by morphological and spectral type in the COSMOS field, identified as quiescent galaxies those with a dereddened color  $(\text{NUV} - r^+) > 3.5$  and consequently having  $\log(\text{sSFR}/\text{Gyr}^{-1}) < -2$ . Mignoli et al. (2009), analyzing the zCOSMOS sample, found that strong and weak line emitters can be well divided by an  $EW_0([\text{OII}]) = 5 \text{ \AA}$ . Combining this information, we therefore identified  $\log(\text{sSFR}/\text{Gyr}^{-1}) < -2 \cap EW_0(\text{H}\alpha \text{ or } [\text{OII}]) < 5 \text{ \AA}$  as the region characteristic of quiescent galaxies in this plot (the non-dashed area).

The quiescent galaxies and the red & passive ETGs samples present, by definition, no tail at high sSFR and EWs, respectively. From the plot, we find that the color-selected samples (red UVJ and red-sequence) and the morphological selected sample instead display a marked percentage of galaxies placed at both high sSFR and EWs, both at low and high redshifts. While the interpretation of intermedi-



**Fig. 2.**  $(U - B)_{\text{rest}}$ -mass diagram. In gray is shown the entire zCOSMOS-20k sample, in violet the morphological ETGs, in light red the red-sequence galaxies, in dark red the red UVJ galaxies, in pink the red SED galaxies, in orange the quiescent galaxies, and in yellow the red & passive ETGs. The upper plot shows the  $(U - B)_{\text{rest}}$ -mass diagram obtained for  $z \leq 0.5$ , and the lower plot shows the diagram obtained for  $z > 0.5$ . The gray hatched area represents the region that falls outside the passive region of the  $(U - B)_{\text{rest}}$ -mass diagram, as defined in Sect. 2.2. The representative errorbar for both quantities is shown in the bottom right corner.



**Fig. 3.**  $(U - V)_{rest} - (V - J)_{rest}$  diagram. In gray is shown the entire zCOSMOS-20k sample, in violet the morphological ETGs, in light red the red-sequence galaxies, in dark red the red UVJ galaxies, in pink the red SED galaxies, in orange the quiescent galaxies, and in yellow the red & passive ETGs. The upper plot shows the diagram obtained for  $z \leq 0.5$ , and the lower plot for  $z > 0.5$ . The gray hatched area represents the region that falls outside the passive region of the UVJ diagram, as defined in Sect. 2.2. The representative errorbar for both quantities is shown in the bottom right corner.

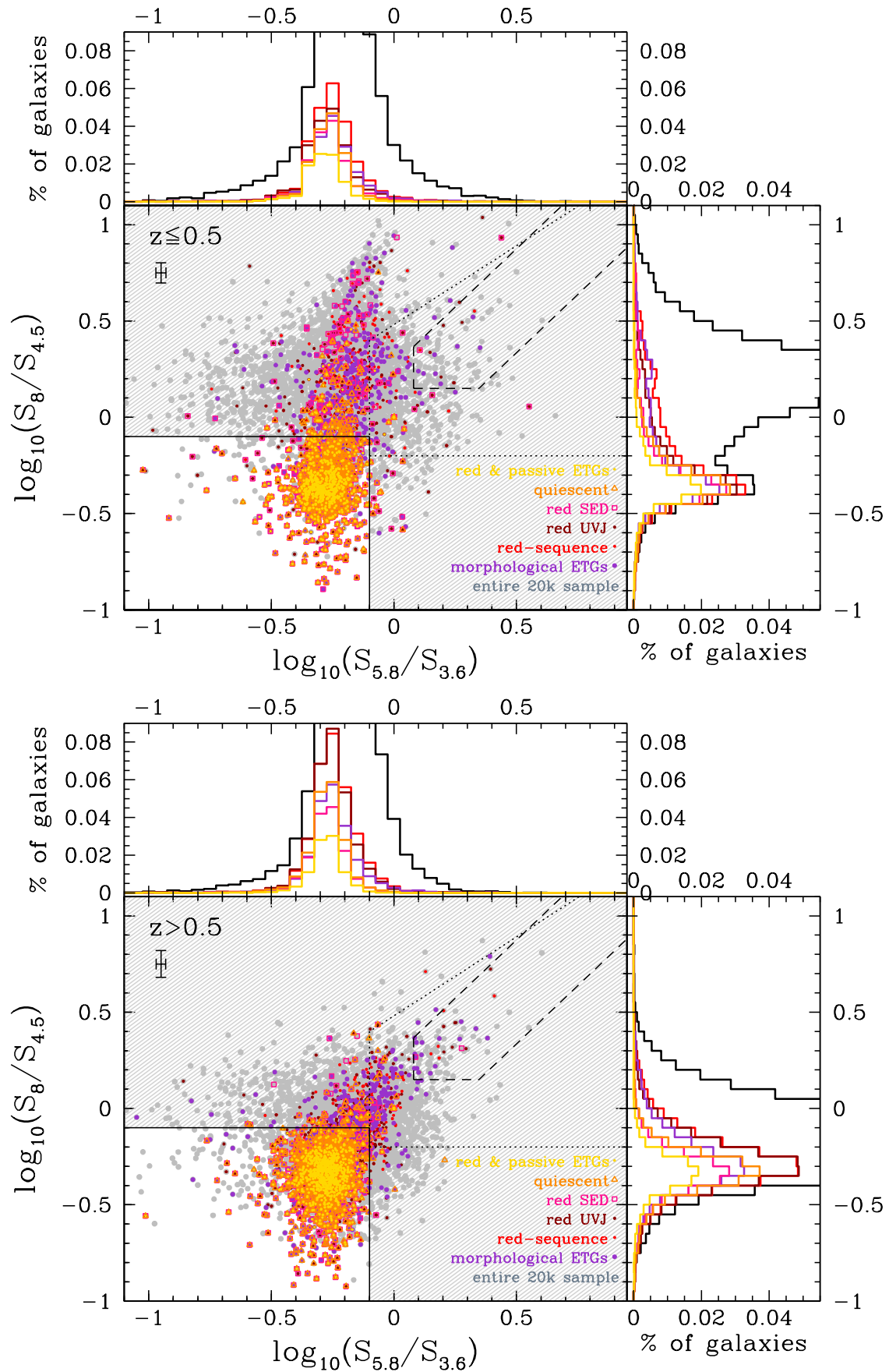


**Fig. 4.**  $\log(S_{8.0}/S_{4.5}) - \log(S_{5.8}/S_{3.6})$  diagram. In gray is shown the entire zCOSMOS-20k sample, in violet the morphological ETGs, in light red the red-sequence galaxies, in dark red the red UVJ galaxies, in pink the red SED galaxies, in orange the quiescent galaxies, and in yellow the red & passive ETGs. The upper plot shows the  $\log(S_{8.0}/S_{4.5}) - \log(S_{5.8}/S_{3.6})$  diagram obtained for  $z \leq 0.5$ , and the lower plot shows the diagram obtained for  $z > 0.5$ . The gray hatched area represents the region that falls outside the passive region of the IRAC color-color diagram, as defined in Sect. 3.1. The dotted lines represent the region defined by Lacy et al. (2004) to identify AGN candidates, and the dashed lines the revised definition by Donley et al. (2012). The representative errorbar for both quantities is shown in the bottom right corner.

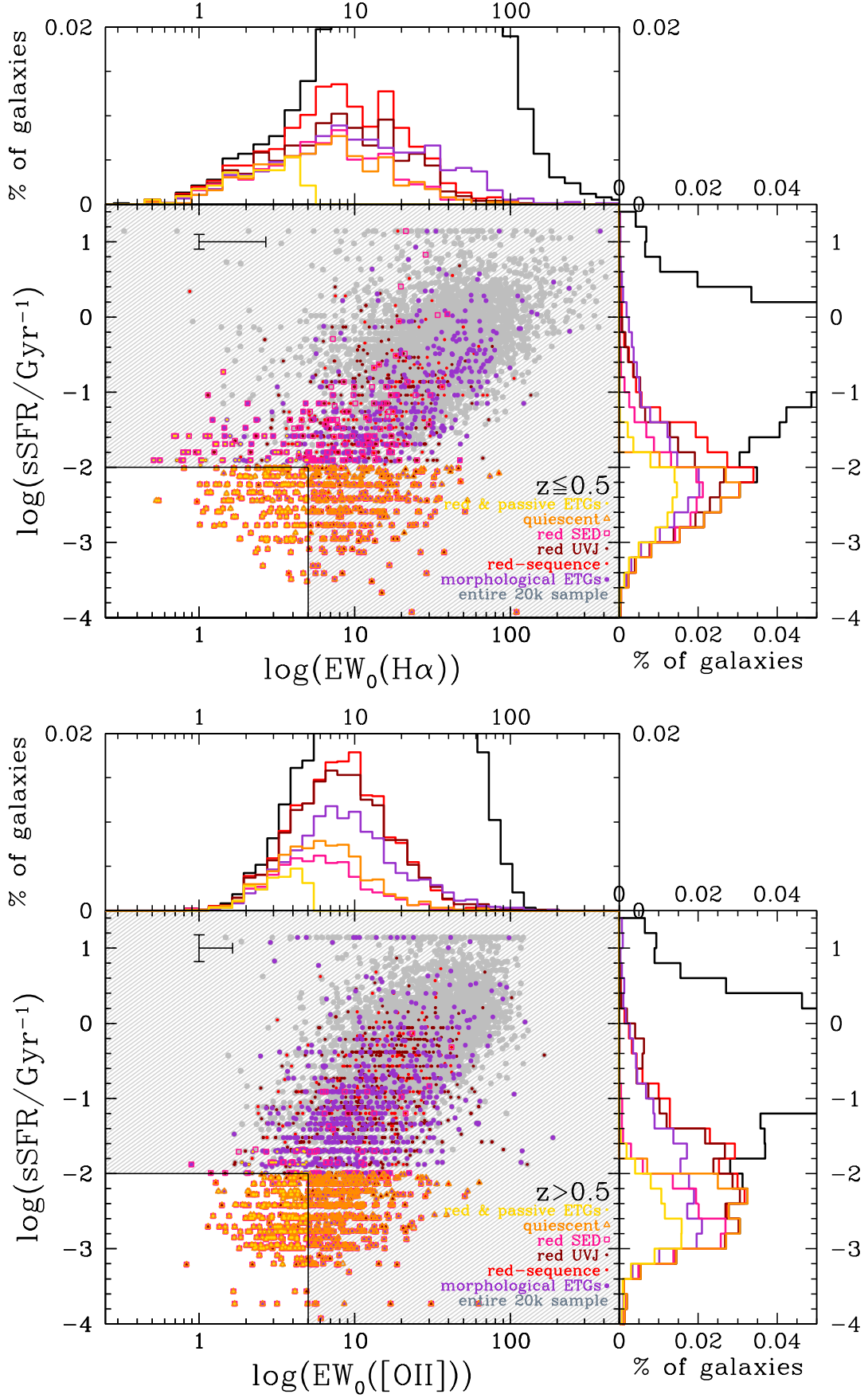


**Fig. 5.** sSFR- $\text{EW}_0([\text{OII}]/\text{H}\alpha)$  diagram. In gray is shown the entire zCOSMOS-20k sample, in violet the morphological ETGs, in light red the red-sequence galaxies, in dark red the red UVJ galaxies, in pink the red SED galaxies, in orange the quiescent galaxies, and in yellow the red & passive ETGs. The upper plot shows the sSFR- $\text{EW}_0(\text{H}\alpha)$  diagram obtained for  $z \leq 0.5$ , and the lower plot shows the sSFR- $\text{EW}_0([\text{OII}])$  diagram obtained for  $z > 0.5$ . The representative errorbar for both quantities is shown in the upper left corner.

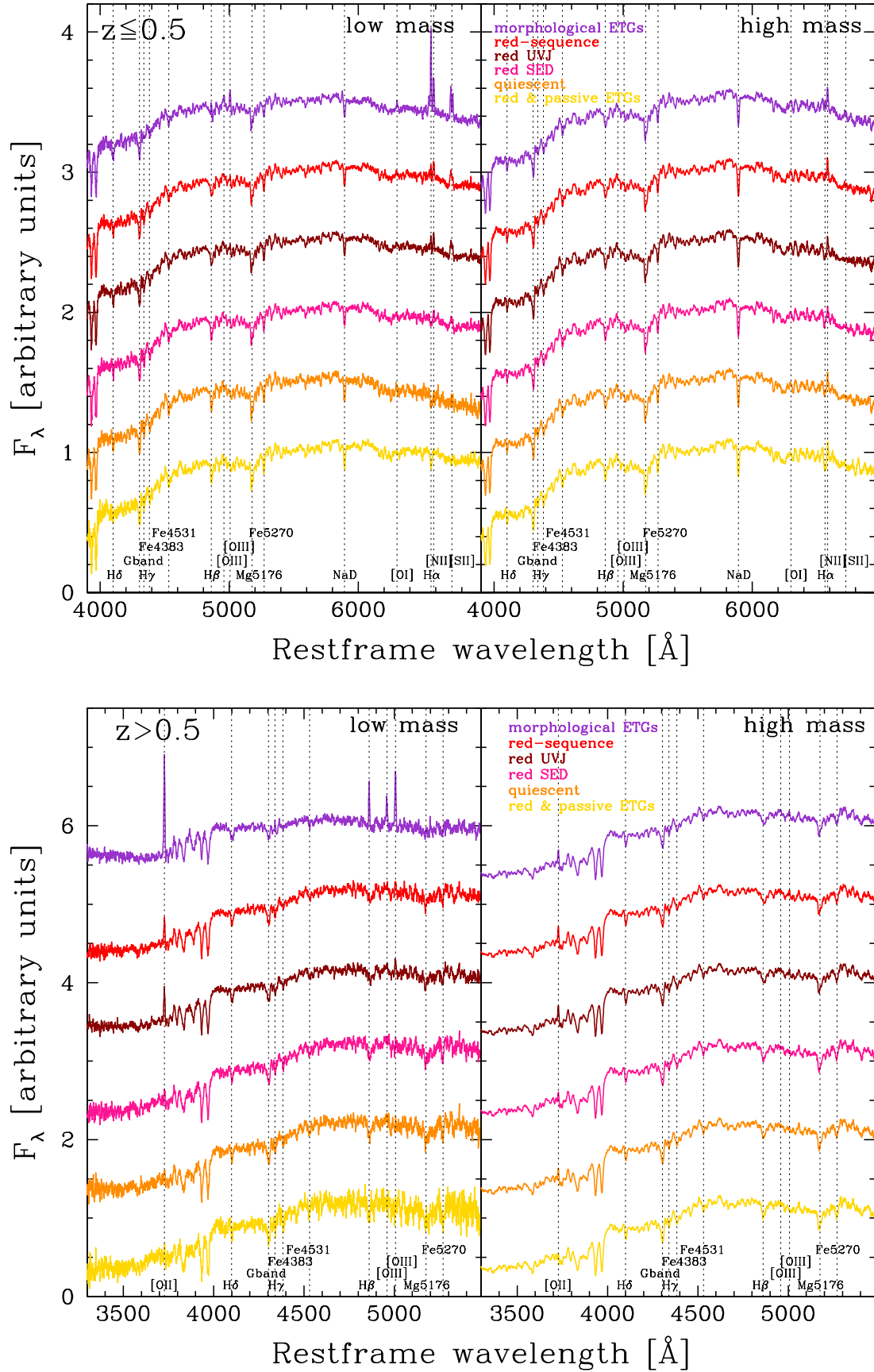


**Fig. 6.** Median stacked spectra obtained for  $z \leq 0.5$  (upper plot) and  $z > 0.5$  (lower plot); the spectra have been evaluated in the low-mass bin ( $\log(\mathcal{M}/M_\odot) < 10.25$ , left panels) and in the high-mass bin ( $\log(\mathcal{M}/M_\odot) > 10.75$ , right panels). In violet are shown the morphological ETGs, in light red the red-sequence galaxies, in dark red the red UVJ galaxies, in pink the red SED galaxies, in orange the quiescent galaxies, and in yellow the red & passive ETGs.

ate values of emission lines in terms of star formation (see for example Yan et al., 2006; Yan & Blanton, 2012) is not straightforward, especially in the presence of a low level of sSFR, the concomitant higher level of sSFR clearly indicates a higher level of star formation with respect to the bulk of the population, which lies in the passive region defined above.

We have also analyzed the stacked median spectra of all samples. In order to disentangle mass and redshift effects, in Fig. 6 we plotted only the median spectra for the low- ( $\log(\mathcal{M}/M_{\odot}) < 10.25$ ) and high-mass ( $\log(\mathcal{M}/M_{\odot}) > 10.75$ ) subsamples, in the low- and high-redshift regimes. At both high and low redshift, several emission lines are clearly detectable for most samples. However, one of the most striking result is that emission lines disappear when passing from the low-mass to the high-mass regime. This represents noticeable evidence that this population is more quenched than the other. We further inspect this trend in Sect. 4.2.

The morphological ETGs present the strongest emission lines, especially at low masses. At high redshift, strong emission lines in [OII],  $H\beta$ , and [OIII] are found. At low redshift, the measured ratios between [NII] $\lambda 6583/H\alpha$  and [OIII] $\lambda 5007/H\beta$  populate the star-forming region in the BPT diagram (Baldwin, Phillips & Terlevich, 1981). This indicates a significant star formation, in particular if we consider that we are analyzing median spectra (see also Pozzetti et al., 2010).

All the other samples show spectra with more typical passive continua, with the presence of faint emission lines in [OII] and  $H\alpha$  only for the red UVJ and red-sequence galaxy samples. At high masses, we find no traces of significant emission lines, and all the spectra show features and continua typical of passively evolving galaxies; this indicates a possible mass dependence that will be further analyzed in Sect. 4.2. In particular, we notice small [OII] emission lines in most spectra at high redshifts, which, however, is compatible with not being caused by star-formation activity (see Yan et al., 2006; Yan & Blanton, 2012, and the discussion of Sect. 4.1). At low redshift, we note that all spectra present a detectable [NII] line (and often also [SII]), but no sign of  $H\alpha$ , probably due to the fact that the  $H\alpha$  emission line is hidden by the corresponding absorption line.

### 3.3. Morphological properties

To study in detail the morphological properties, we analyzed the ZEST (Scarlata et al., 2007) types of the various samples. While for almost all the samples a large fraction of galaxies have an E/S0 morphology (a clear example is shown in Fig. 7), there is a significant fraction, which depends on the adopted selection criteria, of galaxies with clearly spiral/irregular morphologies (see Fig. 8). Despite the evident correspondence between the bimodality in photometric properties and in morphological types, all the samples are contaminated by late-type morphologies: this suggests that the color and the morphological transformation are two distinct processes taking place at different times in the life of a galaxies.

This result confirms what was found with independent methods by other analyses (see, for example, Pozzetti et al., 2010; Ilbert et al., 2010), i.e., that the morphological transformation from late-type to early-type galaxies is a process which intervenes on different timescales than the color

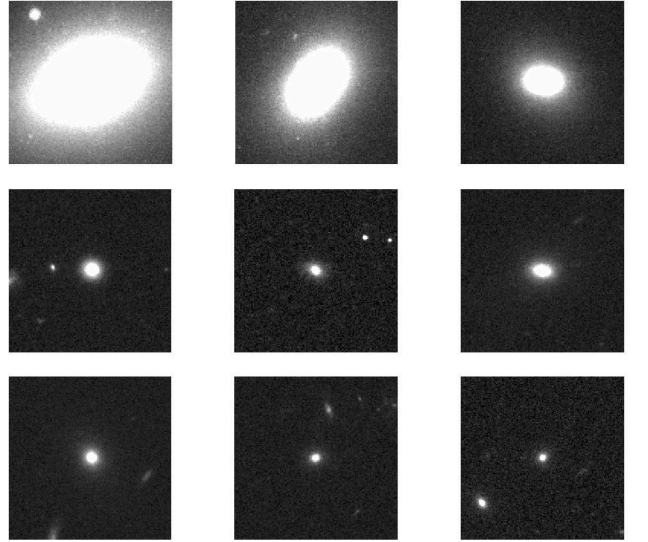


**Fig. 7.** Examples of ACS morphology for a subsample of the red & passive ETGs with elliptical morphologies. The galaxies are shown at increasing redshift from upper left to lower right, from  $z = 0.0791$  to  $z = 0.9302$ .

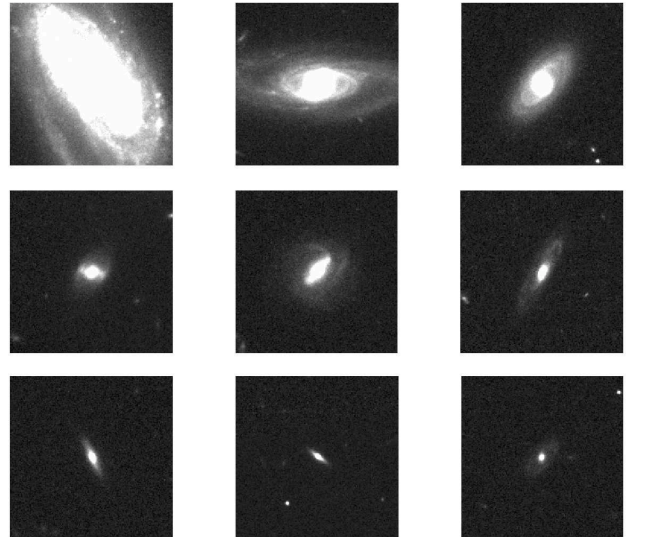


**Fig. 8.** Examples of ACS morphology for a subsample of the red & passive ETGs with very late-type morphologies, found for less than 10% of the overall sample. The galaxies are shown at increasing redshift from upper left to lower right, from  $z = 0.0998$  to  $z = 0.834$ .

transformation. As a result, it is likely for a galaxy, even if it has already stopped its star-formation activity, not to have an elliptical morphology. In contrast to other properties, it is thus improper to consider those galaxies as star-forming contaminants, and the presence of morphologically late-type galaxies will be considered separately.

## 4. Results

To quantitatively estimate which is the best (i.e., the least biased as possible) selection criterion, we estimated the level of contamination by examining different observables, considering colors, sSFR, spectroscopic features, and visual morphology. Of course, as anticipated, these criteria should not be too restrictive because otherwise we trade purity for a poor completeness.

By definition, the less contaminated criterion will be the red & passive ETGs since it uses all the possible information available for these galaxies. However, in the context of many galaxy surveys, it is of utmost interest to also identify a sample that is at the same time the most economic as possible (in terms of information used) and as less biased as possible (in terms of star-forming outliers). To carry on this analysis, it is necessary not only to consider the percentage of contaminants present in each sample but also their absolute values, as well as the dependence on the redshift and on the stellar mass of the contamination.

### 4.1. Study of the contamination

The criteria adopted to define a contaminant are complementary to the ones used to select the various samples of passive galaxies and are described as:

- *blue*  $(U - B)_{\text{rest}}$  colors:

$$(U - B)_{\text{rest}} < 1.10 + 0.075 \log\left(\frac{\mathcal{M}}{10^{10} \mathcal{M}_{\odot}}\right) - 0.18 z$$

- *nonpassive UVJ* colors:

$$(U - V)_{\text{rest}} < 0.88 \times (V - J)_{\text{rest}} + 0.69 \quad [+0.59 \text{ for } z > 0.5]$$

$$\cup (U - V)_{\text{rest}} < 1.3 \cup (V - J)_{\text{rest}} > 1.6$$

- *nonpassive IRAC* colors:

$$\log(S_{8.0}/S_{4.5}) > -0.1$$

$$\cup \log(S_{5.8}/S_{3.6}) > -0.1$$

- *high sSFR*:

$$\log(\text{sSFR}) > -2 \text{ [Gyr}^{-1}\text{]}$$

- *presence of emission lines*:

$$\text{EW}_0(\text{H}\alpha) > 5 \text{ \AA} \text{ (if } z \leq 0.5\text{)}$$

$$\text{or } \text{EW}_0([\text{OII}]) > 5 \text{ \AA} \text{ (if } z > 0.5\text{)}$$

- *nonelliptical morphology*: ZEST type later than E/S0.

For each mass and redshift subsample of the various samples defined in Sect. 2.2, we estimated the median  $(U - B)_{\text{rest}}$  color, sSFR, IRAC colors, restframe equivalent width of H $\alpha$  ([OII] for  $z > 0.5$ ), and morphology of the just defined *contaminant*, as well as the percentage of contamination relative to each subsample. These values are reported in Tab. 2.

As discussed above for the morphology, the spectroscopic properties would also be worth a dedicated discussion, since it is not straightforward that a weak [OII] or H $\alpha$  emission line is symptomatic of star-formation activity (Yan et al., 2006; Yan & Blanton, 2012). However, for simplicity we address as a contaminant a galaxy having any of

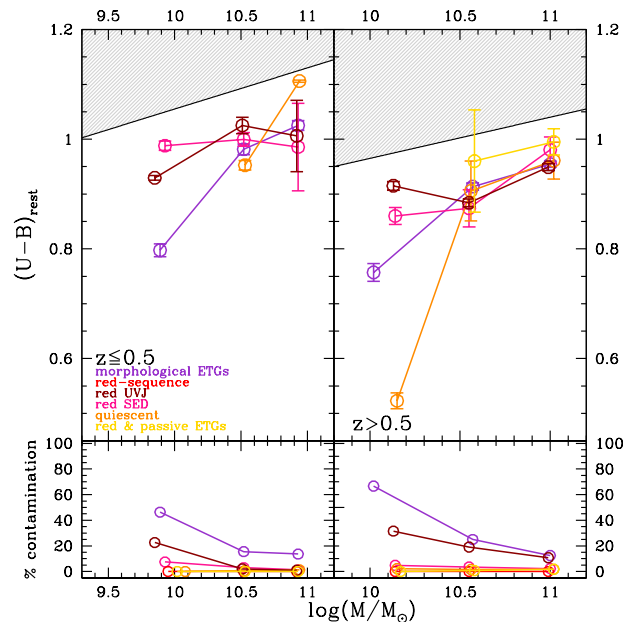


**Fig. 9.** Median  $(U - B)_{\text{rest}}$  color (upper panel) and relative percentage (lower panel) as a function of stellar mass of galaxies with blue colors, i.e.,  $(U - B)_{\text{rest}} < 1.10 + 0.075 \log\left(\frac{\mathcal{M}}{10^{10} \mathcal{M}_{\odot}}\right) - 0.18 z$ , for the different selection criteria (in violet the morphological ETGs, in light red the red-sequence galaxies, in dark red the red UVJ galaxies, in pink the red SED galaxies, in orange the quiescent galaxies, and in yellow the red & passive ETGs). The errorbars represent the error on the median.

these properties considered non-standard for an early type and examine each one individually.

For each considered property, a trend with stellar mass is evident for all the samples, with a decreasing percentage of contaminants with increasing mass. This effect will be analyzed in the following section. Below we discuss separately the contamination in optical and IRAC colors, in sSFR, in spectroscopy, and in morphology.

**Blue  $(U - B)_{\text{rest}}$  colors.** In Sect. 3.1 we have shown the  $(U - B)_{\text{rest}}$ -mass diagram for all the samples, proving that, given the adopted selection criteria, almost all the selected galaxies lie in the red sequence, with minor tails extending in the blue cloud. As a consequence, the number of outliers with clearly blue colors are a minor percentage, typically  $\lesssim 5\%$  for all criteria (except morphological and red UVJ galaxies) at both low and high redshift. Moreover, as can be inferred from Tab. 2, this small fraction of blue outliers has relatively red colors, very close to the considered separation between red sequence and blue cloud. In contrast, morphological ETGs display a substantial percentage of galaxies,  $\sim 12 - 65\%$  depending on the redshift range and on the mass regime, with a median  $(U - B)_{\text{rest}}$  color bluer with respect to the contaminants present in the other samples. This fact testifies that even if a correlation exists between photometric properties and morphology of passive galaxies, it is not a one-to-one correlation, and a considerable number of blue ellipticals coexist with their more standard

red counterparts (see also Tasca et al., 2009). Also the red UVJ sample presents a significant contamination,  $\sim 30\text{-}10\%$  depending on the redshift range and on the mass regime. This is probably due to the fact that the color cuts defined by Williams et al. (2009) do not seem to reproduce well the observed bimodality in the UVJ diagram (as it can be seen by Fig. 3), with tails evident in the blue part of the  $(U - V)_{\text{rest}}$  histogram. However, the median color of the contaminant is, as in most of the previous cases, very close to the adopted definition of red sequence. All these data are reported in Tab. 2 and shown in Fig. 9.

**Nonpassive UVJ colors.** For the UVJ color-color diagram, we considered as a contaminant a galaxy with  $(U - V)_{\text{rest}}$  and  $(V - J)_{\text{rest}}$  colors outside the region defined by Williams et al. (2009). Therefore we just estimated the percentage of these galaxies for each selection criterion; we refer to Sect. 3.1 for the discussion about where those contaminants lie in the UVJ color-color diagram.

This analysis confirms the results just discussed for the color-mass diagram: the quiescent galaxies, red SED galaxies, and red & passive ETGs fit almost perfectly to the passive region in the UVJ diagram, with a percentage of contaminants always below 20% at low redshift and below 5% at high redshift. The percentage of contaminants is slightly higher for the red-sequence sample, around 10-30%, and this fact demonstrates that the cut defined by Peng et al. (2010) in the  $(U - B)_{\text{rest}}$  is also not optimal in dividing passive and star-forming galaxies. As in the previous analysis, the morphological ETGs are the sample with the highest contamination in UVJ colors, around 12-65% depending on the redshift and mass ranges.

**Nonpassive IRAC colors.** The study of the IRAC colors allows a clearer estimate of the presence of star-forming contaminants since these bands were not directly used to define ETG samples (they were used in the red SED galaxies, but together with all the other photometric bands for the best fit to the SEDs). We considered as a contaminant a galaxy falling outside the passive IRAC selection defined in Sect. 3.1. Therefore, since it is possible for such galaxy to have a redder  $S_{5.8}/S_{3.6}$  color or a redder  $S_{8.0}/S_{4.5}$  color, or both, as for the UVJ case, we just estimated the percentage of these galaxies for each selection criterion and refer to Sect. 3.1 for the discussion about where those contaminants lie in the IRAC color-color diagram.

The morphological ETGs are the sample with the higher percentage of contamination,  $\sim 20\text{-}75\%$  depending on the mass and redshift range. Similar to the case of the sSFR, the red UVJ and the red-sequence galaxies are more biased, with  $\sim 25\text{-}55\%$  (depending on the mass range) of the sample not classified as passive for the IRAC color-color criterion at  $z \leq 0.5$  and  $\sim 10\text{-}50\%$  at  $z > 0.5$ . Apart from the red & passive ETGs sample, with a contamination of  $\sim 5 - 25\%$  at low redshift and of  $\sim 2 - 40\%$  at high redshift (from the lowest to the highest masses), the purest samples are the quiescent and the red SED galaxies ( $\sim 10 - 45\%$  at low redshift and  $\sim 3 - 45\%$  at high redshift).

**High sSFR.** Considering the sSFR, the morphological ETGs are the sample with the most extended tails ( $\sim 30\text{-}90\%$ ), with median values up to  $\log(\text{sSFR}/\text{Gyr}^{-1}) \sim -0.6$ ,

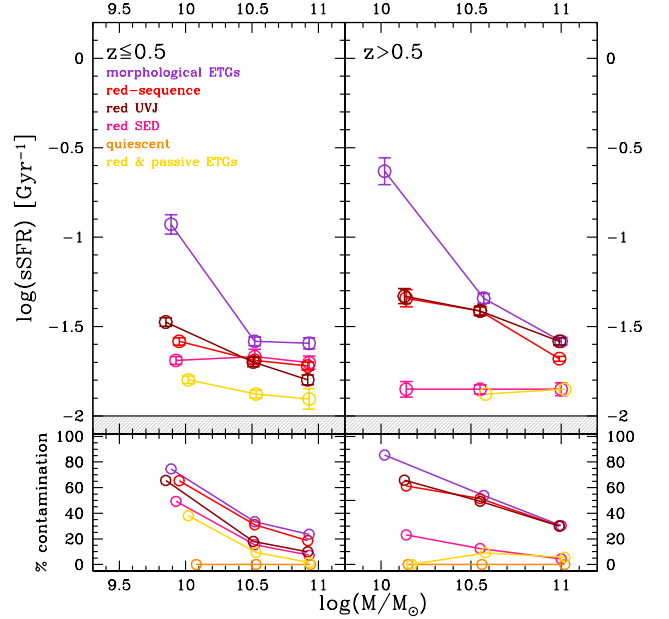


**Fig. 10.** Median  $\log(\text{sSFR}/\text{Gyr}^{-1})$  (upper panel) and relative percentage (lower panel) as a function of stellar mass of galaxies with high sSFR, i.e.,  $\log(\text{sSFR}/\text{Gyr}^{-1}) > -2$ , for the different selection criteria (in violet the morphological ETGs, in light red the red-sequence galaxies, in dark red the red UVJ galaxies, in pink the red SED galaxies, in orange the quiescent galaxies, and in yellow the red & passive ETGs). The errorbars represent the error on the median.

corresponding to a star-formation activity  $\sim 25$  times higher with respect to the adopted definition of quiescent (i.e.,  $\log(\text{sSFR}/\text{Gyr}^{-1}) < -2$ ). Both red UVJ and red-sequence samples represent an intermediate case, with a median  $\log(\text{sSFR}/\text{Gyr}^{-1}) \sim -1.5/-1.7$  for the contaminants ( $\sim 3$  times more star-formation activity than the assumed quiescent limit), and a percentage of contamination  $\sim 20\text{-}65\%$ , depending on the mass range. The less biased samples (the quiescent sample is by definition not biased with respect to this parameter) are the red SED and the red & passive ETGs ones, having median values of sSFR much closer to the quiescent limit and a percentage of contamination in most cases  $\lesssim 15\%$ . All these data are reported in Tab. 2 and shown in Fig. 10.

**Presence of emission lines.** We estimated the median equivalent width of  $\text{H}\alpha$  at  $z \leq 0.5$ , and  $[\text{OII}]$  at  $z > 0.5$  for the galaxies with significant emission lines (i.e.,  $> 5 \text{ \AA}$ ) in each sample; the results are reported in Tab 2 and shown in Fig. 11. The sample with the strongest emission lines is the morphological ETGs, with median equivalent widths up to  $\sim 30 \text{ \AA}$  and with a percentage of contamination going from 55-70% to 35%, depending on the mass range. The red UVJ and the red-sequence samples show a similar and smaller contamination, both in percentage ( $\sim 40\%$ ) and median value ( $\sim 15\text{-}10 \text{ \AA}$ ). The less contaminated samples are the quiescent and the red SED galaxies: the percentage of galaxies with emission lines  $> 5 \text{ \AA}$  is  $\sim 30\%$  at low redshift

	$z \leq 0.5$						$z > 0.5$					
	low-mass		med-mass		high-mass		low-mass		med-mass		high-mass	
	median	%	median	%	median	%	median	%	median	%	median	%
<b>blue <math>(U - B)_{\text{rest}}</math> colors</b>												
morphology	0.80	46.3%	0.98	15.5%	1.03	13.6%	0.76	66.7%	0.91	25%	0.95	12.4%
red-sequence	–	–	–	–	–	–	–	–	–	–	–	–
red UVJ	0.93	22.6%	1.03	2%	1.01	0.9%	0.91	31.5%	0.88	19.2%	0.95	10.8%
red SED	0.99	7.5%	1.00	3%	0.98	1.3%	0.86	4.8%	0.87	3.6%	0.98	2.3%
passive	–	0.0%	0.95	0.8%	1.11	1.3%	0.52	2.2%	0.91	1.6%	0.96	1.7%
red & passive ETGs	–	0.0%	–	0.0%	–	0.0%	–	0.0%	0.96	0.7%	1	1.8%
<b>nonpassive UVJ colors</b>												
morphology	46.6%		30.4%		32.7%		63%		25.7%		12.1%	
red-sequence	23.1%		28.2%		29.5%		23.3%		24.3%		12.7%	
red UVJ	–		–		–		–		–		–	
red SED	8.9%		16.5%		18.2%		5.8%		5.6%		4.6%	
quiescent	1.4%		13.6%		22.2%		3.3%		3.7%		3.6%	
red & passive ETGs	3.9%		13.2%		10.8%		0.0%		1.1%		1.5%	
<b>nonpassive IRAC colors</b>												
morphology	60.1%		26.6%		26.0%		60.4%		23.3%		7.6%	
red-sequence	55.3%		26.1%		25.1%		51.3%		21.6%		8.4%	
red UVJ	55.2%		13.6%		9.6%		49.6%		18.5%		7.2%	
red SED	44.7%		14.4%		11%		41.4%		10.9%		2.6%	
quiescent	29.6%		8.6%		14.4%		43.5%		9.4%		2.5%	
red & passive ETGs	25.2%		7%		5.2%		38.9%		3.2%		1.6%	
<b>high sSFR</b>												
morphology	-0.93	74.6%	-1.58	33.3%	-1.59	23.7%	-0.63	85.4%	-1.34	53.8%	-1.58	30.3%
red-sequence	-1.58	65.4%	-1.69	31.1%	-1.72	18.7%	-1.34	61.2%	-1.41	51.4%	-1.68	30.3%
red UVJ	-1.48	65.6%	-1.70	18%	-1.80	9.9%	-1.3	65.8%	-1.41	49.3%	-1.58	30.1%
red SED	-1.69	49.3%	-1.67	15.4%	-1.70	7.2%	-1.85	12.4%	-1.85	13.2%	-1.85	4.4%
quiescent	–	–	–	–	–	–	–	–	–	–	–	–
red & passive ETGs	-1.80	38.1%	-1.88	9.5%	-1.91	1.6%	–	0.0%	-1.88	9.1%	-1.85	5.6%
<b>presence of emission lines</b>												
morphology	-29.2	55.4%	-12.3	35.9%	-11.6	38.6%	-23.1	68.2%	-10.3	45.6%	-9.1	38%
red-sequence	-14.3	41.8%	-11	33.8%	-10.9	36.3%	-13.4	39.2%	-10.5	43.3%	-9.2	38.5%
red UVJ	-14.0	42.1%	-10.8	26.6%	-10.1	28.7%	-16.5	46.2%	-10.7	41.7%	-9.2	37.9%
red SED	-12.2	30.4%	-9.2	27.8%	-9.5	28.9%	-8.6	10.75%	-7.9	21.6%	-8.3	23%
quiescent	-12.0	20.7%	-9.4	25.9%	-10.4	31.4%	-13.4	14.1%	-8.3	21.2%	-8.4	26.6%
red & passive ETGs	–	–	–	–	–	–	–	–	–	–	–	–
<b>nonelliptical morphology</b>												
morphology	–	–	–	–	–	–	–	–	–	–	–	–
red-sequence	2.1	60.8%	2.1	39%	2.1	22.8%	2.1	67.2%	2.1	55.4%	2.1	31.5%
red UVJ	2.1	60.6%	2.1	31%	2.1	15.2%	2.1	67.3%	2.1	52.7%	2.1	29.9%
red SED	2.1	51.9%	2.1	30%	2.1	18.9%	2.1	59.6%	2.1	44.8%	2.1	22.9%
quiescent	2.1	50.2%	2.1	31.4%	2.1	18.6%	2.1	63%	2.1	45.7%	2.1	23.7%
red & passive ETGs	2.1	34.8%	2.1	25.7%	2.1	11.3%	2.1	77.8%	2.1	40.7%	2.1	15.1%

**Table 2.** Contamination of the different samples of passive galaxies as a function of stellar mass and redshift. The table reports the median values of colors, sSFR, equivalent widths and morphology for the galaxies having blue colors, high specific star formation rates, significant emission lines and late-type morphologies as defined in Sect. 4.1, and the percentage relative to each subsample. The low-mass bin refers to  $\log(\mathcal{M}/M_{\odot}) < 10.25$ , the med-mass bin to  $10.25 < \log(\mathcal{M}/M_{\odot}) < 10.75$ , and the high-mass bin to  $\log(\mathcal{M}/M_{\odot}) > 10.75$ . As defined in the text, the emission lines reported are the median restframe equivalent widths (in units of  $\text{\AA}$ ) of  $\text{H}\alpha$  for  $z \leq 0.5$  and of  $[\text{OII}]$  for  $z > 0.5$ ; by convention, the emission lines are quoted with negative values.

and slightly smaller ( $\sim 20\%$ ) at higher redshift, with median values closer to the adopted cut ( $\sim 8\text{--}10 \text{\AA}$ ).

Many works have already shown the presence of emission lines in the spectra of red/passive galaxies. However, given their line ratios, these are usually classified as LINERS (low-ionization nuclear emission-line regions, Heckman, 1980), or with a LINER-like emission (e.g., see

Phillips et al., 1986; Yan et al., 2006; Annibali et al., 2010; Yan & Blanton, 2012). As summarized by Annibali et al. (2010), the most probable mechanisms proposed to produce such lines are a low accretion-rate AGN, fast shocks, or photoionization by old post-asymptotic giant branch (PAGB) stars. More recent studies favor the last option (see also Yan & Blanton, 2012). It is beyond the aim of this paper

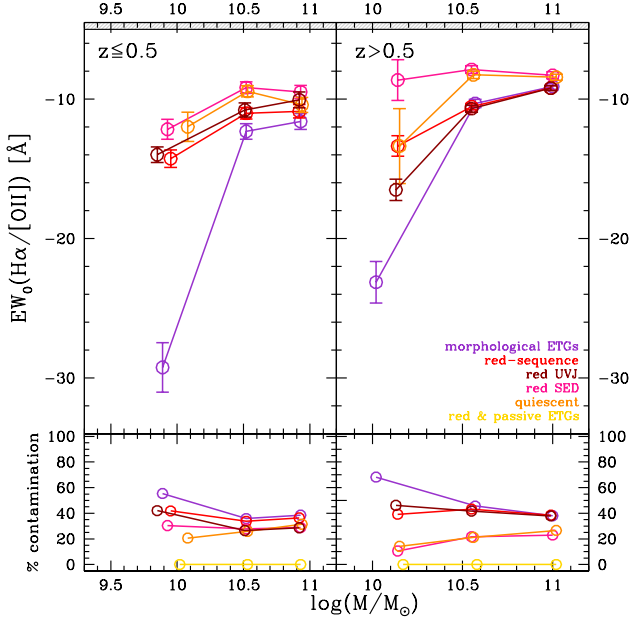


**Fig. 11.** Median  $EW_0(H\alpha)$  (upper panel;  $EW_0([OII])$  if  $z > 0.5$ ) and relative percentage (lower panel) as a function of stellar mass of galaxies with significant emission lines, i.e.,  $EW_0(H\alpha) > 5 \text{ \AA}$  (if  $z \leq 0.5$ ) and  $EW_0([OII]) > 5 \text{ \AA}$  (if  $z > 0.5$ ), for the different selection criteria (in violet the morphological ETGs, in light red the red-sequence galaxies, in dark red the red UVJ galaxies, in pink the red SED galaxies, in orange the quiescent galaxies, and in yellow the red & passive ETGs). The errorbars represent the error on the median. By convention, the emission lines are quoted with negative values.

to analyze in detail the source of ionization in this population of galaxies; what we wanted to stress here is that in this population of galaxies weak emission lines do not necessarily trace star-formation activity, especially if the sSFR as found from the SED-fitting does not confirm a significant star formation. On the other hand, the stronger emission lines found in morphological ETGs should actually trace star-formation activity, as confirmed by the ratio with the other significant emission lines ( $H\beta$ ,  $[NII]\lambda 6583$ ,  $[OII]\lambda 5007$ ).

**Nonelliptical morphology.** The median morphology estimated for the galaxies not matching an elliptical template is equal to a ZEST type = 2.1 in all samples, which corresponds to a bulge-dominated spiral galaxy. This means that for all samples the tail of morphologies is not extended toward very late-type templates. However, all the samples show a high percentage of contamination due to non elliptical-galaxies, with percentages going from  $\sim 60\%$  at low masses to  $\sim 25\text{-}30\%$  at high masses, the less biased sample being the red & passive ETGs one.

This evidence confirms that the color transformation and the morphological transformation from late-type to early-type galaxies are not concomitant processes and that the quenching of the star-formation activity could precede the change in morphological type.

#### 4.2. Contamination as a function of mass

The analysis of the different properties of passive galaxies indicated a clearly evident dependence of the contamination on the stellar mass. Looking at Tab. 2, it is possible to see that the percentage of contamination in almost all the analyzed properties decreases from  $\log(M/M_\odot) < 10.25$  to  $\log(M/M_\odot) > 10.75$  by a factor  $\sim 2\text{-}3$ . Figures 9, 10, and 11 also highlight a mass dependence of the absolute value of the properties of the contaminants in all samples: for example the colors of contaminants are redder by  $\sim 10\text{-}30\%$  at high masses than at low masses and are closer to the red sequence. This trend can also be found in sSFR and equivalent widths of emission lines, with the lower mass bin having a star-formation activity  $\sim 10\%$  higher and emission lines  $\sim 5 \text{ \AA}$  larger than the high-mass bin for all the samples considered, both at high and at low redshift.

From this analysis we found that, irrespective of the adopted selection criterion, an additional stellar mass cut provides a purer sample of passively evolving galaxies, significantly reducing the contamination by star-forming galaxies.

#### 4.3. Contamination as a function of selection criteria

There are different ways to quantify the best method to select a population of passively evolving galaxies. On one hand, it is possible to ask which criterion is least biased by the presence of star-forming outliers, independently of how much information is used. On the other hand, at a fixed percentage of contamination, it is possible to ask which is the most economic criterion in terms of information used. The first will privilege the purity of the sample but has the drawback of requiring a large amount of data to be used. In contrast, the second will be necessarily more contaminated but also of greatest interest in many surveys where less data are available, due to low spectral resolution or limited wavelength coverage.

Needless to say, the purest sample is the one based on the combined selection criterion since the use of photometric, spectroscopic, and morphological information helps to minimize the presence of blue, star-forming galaxies. It provides red and passive galaxies with a color contamination, also in the IRAC colors,  $< 10\%$  for stellar masses  $\log(M/M_\odot) > 10.25$ , both at low and high redshifts. The specific star formation of the outliers ( $\lesssim 10\%$  for  $\log(M/M_\odot) > 10.25$ ) is only  $\sim 20\%$  higher than the chosen passive cut, and the contaminants equivalent widths of emission lines, both  $[OII]$  and  $H\alpha$ , are smaller than  $\sim 10 \text{ \AA}$ .

Apart from this criterion, all the others, except the morphological criterion, are equivalent in terms of requirements since they all need a best fit to the observed SED to obtain stellar masses, SFRs, and/or restframe colors necessary to perform the selection. Among them, the best-performing criteria have proven to be the red SED and the quiescent ones. An analysis of Tab. 2 and Figs. 9, 10, and 11 shows that they have the minimum percentage of contamination in both optical colors ( $\lesssim 5\%$ ), IRAC colors ( $\lesssim 15\%$ ), spectroscopic features ( $\lesssim 30\%$ ), and sSFR ( $\lesssim 15\%$ ). The percentage of contamination is slightly higher than the red & passive ETGs criterion, on average by a factor of  $\sim 2$ , but the absolute values of the properties of contaminants are still compatible with a red, passively evolving population.

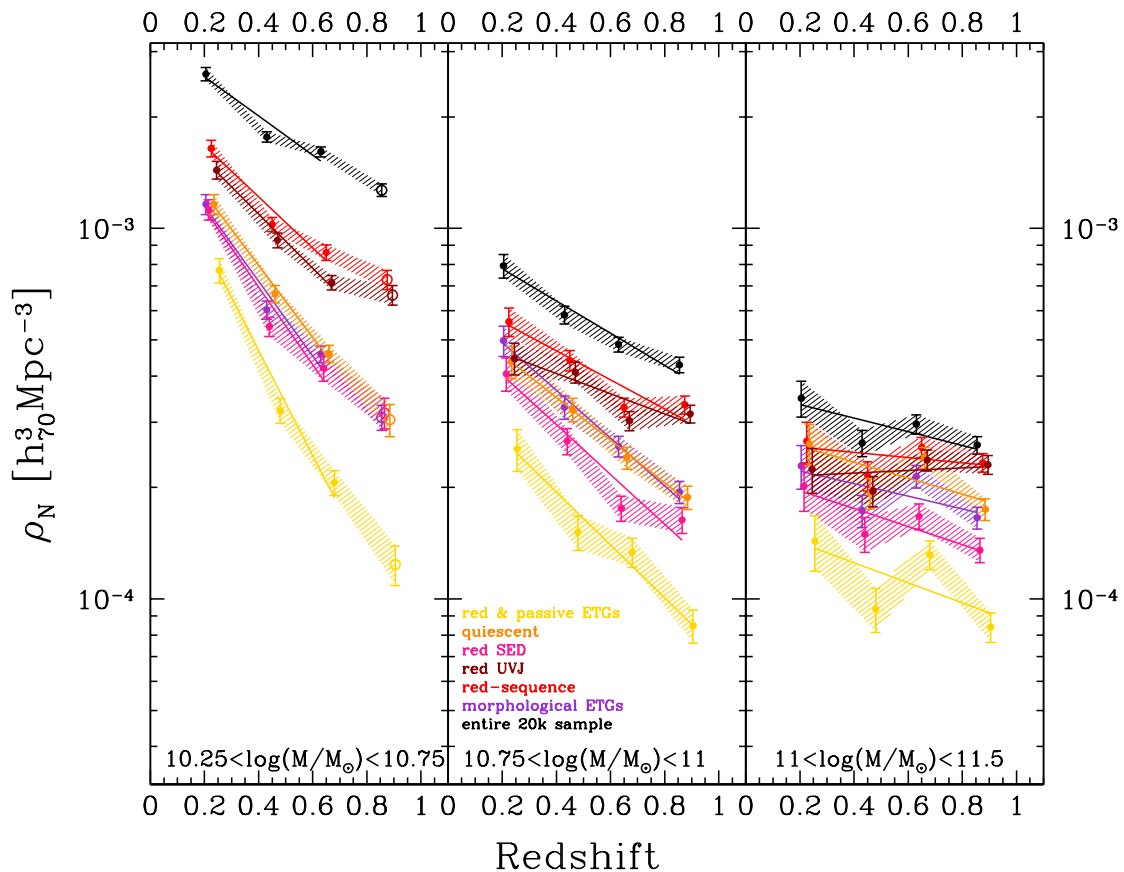


**Fig. 12.** Redshift evolution of the galaxy number density, derived using  $1/V_{\max}$ , for three different mass ranges:  $10.25 < \log(\mathcal{M}/M_{\odot}) < 10.75$  (left panel),  $10.75 < \log(\mathcal{M}/M_{\odot}) < 11$  (central panel) and  $\log(\mathcal{M}/M_{\odot}) > 11$  (right panel). The different colors represent different selection criteria (violet for the morphological ETGs, light red for the red-sequence galaxies, dark red for the red UVJ galaxies, orange for the quiescent galaxies, and yellow for the red & passive ETGs). The lines represent the fit to the observed  $\log(\rho_N(z))$  relation. The open points represent the lower limits where the survey is not complete.

#### 4.4. Number density

For all the samples, we estimated the galaxy stellar mass functions using the nonparametric  $1/V_{\max}$  formalism (Schmidt, 1968), from which we derived the number density ( $\rho_N$ ) in three mass bins,  $\log(\mathcal{M}/M_{\odot}) = 10.25 - 10.75, 10.75 - 11, 11 - 11.5$ . The redshift evolution of the galaxy number density is shown in Fig. 12. As a comparison, we also reported the number density in the same mass range for the parent zCOSMOS-20k sample. Each relation was fitted using a weighted linear least square minimization, considering only the redshift bins in which the data are complete. The trends are similar for the differently selected samples, even if the normalization is different.

In the lower stellar mass bin, we find a pronounced evolution, with an increase in number densities by a factor  $\sim 2 - 4$  between  $z \sim 0.65$  and  $z \sim 0.2$ . At stellar masses  $10.75 < \log(\mathcal{M}/M_{\odot}) < 11$ , we still find a noticeable evolution, with an increase by a factor  $\sim 2-3$  between  $z \sim 0.85$  and  $z \sim 0.2$ . At higher masses,  $11 < \log(\mathcal{M}/M_{\odot}) < 11.5$ , the evolution is much less pronounced, with a percentage increase in number density of  $\sim 10-50\%$  in the entire redshift range.

The stronger increase in the number density of low/intermediate-mass passive galaxies with respect to massive and passive galaxies is a clear indication of mass-assembly “downsizing” (Fontana et al., 2004; Drory et al., 2005; Bundy et al., 2006; Cimatti et al., 2006; Thomas et al., 2010; Pozzetti et al., 2010; Moresco et al., 2010), with more massive galaxies having assembled their mass at higher redshifts and already being in place at  $z \sim 1$ . The result of this analysis is in agreement with many other works: Scarlata et al. (2007) studying ETGs in the COSMOS field found no traces of significant evolution in the number density of bright ( $\sim L > 2.5L^*$ ) ETGs, with a maximum increase of  $\sim 30\%$  from  $z \sim 0.7$  to  $z \sim 0$  when allowing for different SFHs and cosmic variance; Pozzetti et al. (2010) found an almost negligible evolution in the number density of quiescent galaxies in zCOSMOS-10k sample,  $< 0.1$  dex between  $z = 0.85$  and  $z = 0.25$  for  $\log(\mathcal{M}/M_{\odot}) > 11 - 11.5$ ; from the analysis of the UltraVISTA-DR1 sample Ilbert et al. (2013) found that massive galaxies ( $\log(\mathcal{M}/M_{\odot}) > 11.2$ ) do not show any significant evolution between  $0.8 < z < 1.1$  and  $0.2 < z < 0.5$ , while low-mass ones ( $\log(\mathcal{M}/M_{\odot}) \sim 9.5$ ) increase in number density by a factor  $> 5$ . Brammer et al. (2011) analyzed the number density of quiescent galaxies at

$0.4 < z < 2.2$  using the NEWFIRM Medium-Band Survey, and found a strong evolution of  $\log(\mathcal{M}/\mathcal{M}_\odot) > 10.5$  galaxies, a factor  $\sim 10$  from  $z \sim 2$  to  $z \sim 0$ . However, this evolution becomes smaller and comparable with the errorbars at high masses between  $z \sim 1$  and  $z \sim 0.6$ , only  $\sim 20\%$  for  $\log(\mathcal{M}/\mathcal{M}_\odot) > 11$  ( $\sim 10\%$  for  $10.6 < \log(\mathcal{M}/\mathcal{M}_\odot) < 11$ ), therefore it is compatible with our results. Maraston et al. (2012), studying the stellar mass function of BOSS galaxies, find that the galaxy number density above  $\sim 2.5 \cdot 10^{11} M_\odot$  agrees with previous measurements within  $2\sigma$ , with no evolution detected from  $z \sim 0.6$ . Also from the analysis of the VIPERS survey, Davidzon et al. (2013) find a much stronger evolution in the number density of less massive galaxies when compared to less massive ones, with an increase of  $\sim 80\%$  between  $z = 1$  and  $z = 0.6$  for masses  $11 < \log(\mathcal{M}/\mathcal{M}_\odot) < 11.4$  and only of  $\sim 45\%$  between  $z = 1.2$  and  $z = 0.6$  for masses  $\log(\mathcal{M}/\mathcal{M}_\odot) > 11.4$ . Finally, Moustakas et al. (2013) measured the evolution of the stellar mass function from the PRISM MUlti-object Survey and confirmed an evolution by a factor of  $3.2 \pm 0.5$  from  $z = 0.4$  to  $z = 0$  for stellar masses  $9.5 < \log(\mathcal{M}/\mathcal{M}_\odot) < 10$ , by a factor of  $2.2 \pm 0.4$  from  $z = 0.6$  to  $z = 0$  for stellar masses  $10 < \log(\mathcal{M}/\mathcal{M}_\odot) < 10.5$ , and only  $\sim 58\% \pm 9\%$  for stellar masses  $10.5 < \log(\mathcal{M}/\mathcal{M}_\odot) < 11$ .

The comparison, at fixed mass, of the number density of the differently selected passive galaxies is also interesting since it sheds some light on the timescales characteristic of different processes. At masses  $\log(\mathcal{M}/\mathcal{M}_\odot) < 11$ , we find that the number densities of the various samples are well separated, with highest normalization for color-selected ETGs, intermediate for the passive/red-SED/morphologically selected ETGs, and lowest for the red & passive ETGs. This may suggest a scenario during which, at these masses, the first transition that an ETG experiences is a color transformation from blue to red, followed by the quenching of the star formation and by the morphological transformation into ellipticals.

A similar trend is found in the work of Pozzetti et al. (2010), which quantified the timescale of the delay between color and morphological transformation to be around 1-2 Gyr. Some support to this scenario also comes from the work of Ilbert et al. (2010), who find that the stellar mass density of quiescent galaxies is always higher than the one of red elliptical galaxies. Obviously the quantitative estimate of the delay between these processes also depends on the adopted cuts to select ETGs since, for example, a lower/higher cut in sSFR will shift the relation lower/higher.

#### 4.5. Revising the color selection criteria

In Sect. 3.1 and 4.1 we presented and discussed the fact that the red-sequence and the red UVJ samples have a higher contamination, which is also clearly evident by a visual inspection of the color-mass and color-color diagrams. However, we also argued that this higher contamination may be due to the fact that the proposed cut may not be optimal, at least for the zCOSMOS-20k survey.

To address this issue, we decided to study how the colors of the contaminants (as defined in Sect. 4.1) for these two criteria are distributed in the  $(U - B)_{\text{rest}}$  color-mass and UVJ color-color diagrams, respectively, in order to understand if an additional cut is able to further reduce the contamination. In Fig. 13 we show the  $(U - B)_{\text{rest}}$ -mass dia-

gram for the red-sequence galaxies (in gray), highlighting in cyan the galaxies presenting a sSFR or emission lines in excess with respect to the passive cuts defined (i.e., the *contaminants*); Fig 14 shows the same as Fig. 13, but for the  $(U - V)_{\text{rest}} - (V - J)_{\text{rest}}$  diagram and for the case of the red UVJ galaxies. From these plots it is evident that statistically the contaminants have bluer colors and therefore that a refined cut may help to reduce the contamination. In particular from Fig. 14 it is clear that there are specific ranges of colors ( $1.3 < (U - V)_{\text{rest}} < 1.5$ ) where the contaminants represent 100% of the distribution.

We therefore defined two revised color selection criteria, with slightly redder colors: for the  $(U - B)_{\text{rest}}$ -mass diagram:

$$(U - B)_{\text{rest}} > 1.15 + 0.075 \times \log\left(\frac{\mathcal{M}}{10^{10} M_\odot}\right) - 0.18 \times z$$

and for the  $(U - V)_{\text{rest}} - (V - J)_{\text{rest}}$  diagram:

$$\begin{cases} (U - V)_{\text{rest}} > 1.6 \\ (V - J)_{\text{rest}} > 1.6 \\ (U - V)_{\text{rest}} > 0.88 * (V - J)_{\text{rest}} + 0.69 \end{cases} \quad [0 < z < 0.5]$$

$$\begin{cases} (U - V)_{\text{rest}} > 1.5 \\ (V - J)_{\text{rest}} > 1.6 \\ (U - V)_{\text{rest}} > 0.88 * (V - J)_{\text{rest}} + 0.66 \end{cases} \quad [0.5 < z < 1]$$

The empty colored histograms in Figs. 13 and 14 show the distribution of the contaminants with the old definitions, while the shaded colored histograms show the distribution of the contaminants obtained with the new definitions just reported. It is evident how these new color selection criteria help to cut significantly the contaminants with blue colors.

We checked that these new selection criteria provide purer samples than the previous ones. The new red UVJ sample no longer presents significant blue tails in the color-mass diagram, having a contamination compatible with all the other samples. In addition, the percentage of contamination of the new red-sequence sample in the UVJ color-color diagram is reduced from 20-40% to 15-25% at low redshift and from 20-40% to 10-15% at high redshift. However, even if reduced with these new definitions, the contamination in terms of sSFR and presence of emission lines is still higher than the quiescent, red SED, and red & passive ETGs criteria, which continue to behave better than the color criteria in selecting a purer sample of ETGs.

## 5. Summary and conclusions

We have studied the photometric, spectroscopic and morphological properties of six differently selected samples of passive galaxies in order to analyze their contamination in terms of blue/star-forming/nonpassive galaxies. From the zCOSMOS-20k spectroscopic catalog, we extracted a sample based on morphology (3336 “morphological” early-type galaxies), on optical colors (4889 “red-sequence” and 4882 “red UVJ” galaxies), on specific star-formation rate (2937 “quiescent” galaxies), on a best fit to the observed SED (2603 “red SED” galaxies), and on a criterion that combines morphological, spectroscopic, and photometric information (1530 “red & passive early-type galaxies”).

For all the samples, we estimated the  $(U - B)_{\text{rest}}$ -stellar mass diagram, the IRAC color-color plot as defined by Lacy et al. (2004), the sSFR-EW<sub>0</sub>([OII]/H $\alpha$ ) diagram, and

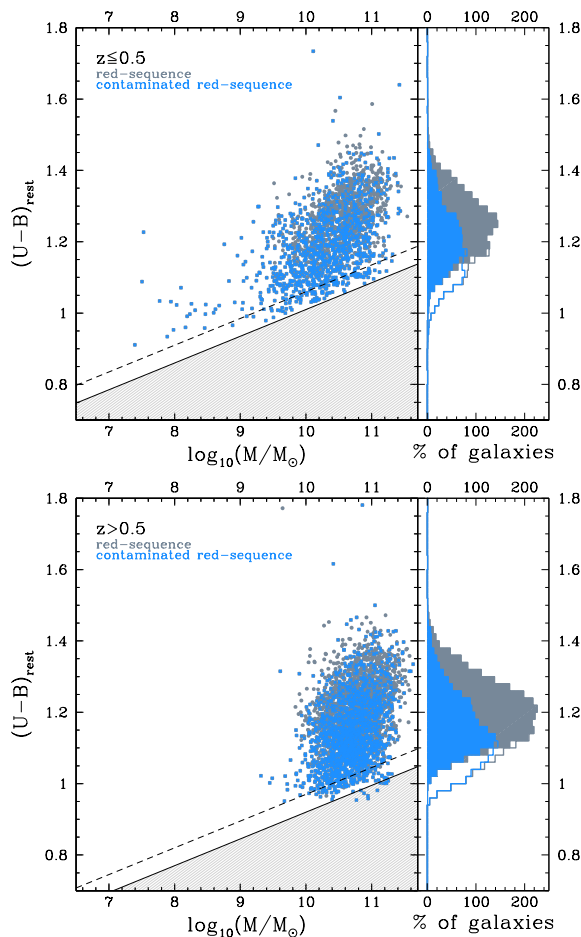


**Fig. 13.**  $(U - B)_{\text{rest}}$ -mass diagram. In gray is shown the original  $(U - B)_{\text{rest}}$ -mass criterion as defined by Peng et al. (2010), and in cyan are highlighted the galaxies presenting a sSFR or emission lines in excess with respect to the passive cuts. The empty cyan histograms show the distribution of the contaminants with the old definitions, while the shaded cyan histograms show the distribution of the contaminants with the new selection criterion as defined in section 4.5. The upper plot shows the diagram obtained for  $z \leq 0.5$ , and the lower plot shows the diagram obtained for  $z > 0.5$ .

the morphological types. We also evaluated the median stacked spectra of these samples to search in detail for the presence of peculiar spectroscopic features that may be a proxy of star-formation activity.

To quantify the contamination of the various samples, for each property we defined a passive cut and studied the percentage of galaxies not fulfilling this cut, as well as the median value of the parameters (color, sSFR,  $EW_0$  of emission lines) involved in each selection. In this way we were also able to study how much these contaminants are close to or far from the assumed passive definition. All these analyses were performed in two redshift bins ( $z \leq 0.5$  and  $z > 0.5$ ) and three stellar mass bins ( $\log(\mathcal{M}/M_\odot) < 10.25$ ,  $10.25 < \log(\mathcal{M}/M_\odot) < 10.75$ , and  $\log(\mathcal{M}/M_\odot) > 10.75$ ).

Our main results are listed below:

- We find that all samples display tails in the star-forming regions of different diagrams, irrespective of the severity

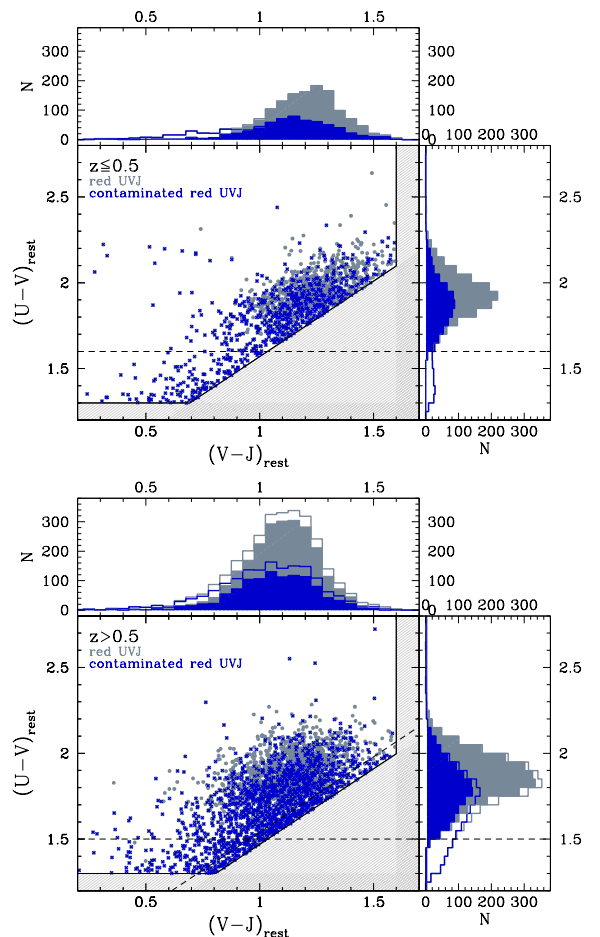


**Fig. 14.**  $(U - V)_{\text{rest}}$ - $(V - J)_{\text{rest}}$  diagram. In gray is shown the original UVJ criterion, as defined by Williams et al. (2009), and in blue are highlighted the galaxies presenting a sSFR or emission lines in excess with respect to the passive cuts. The empty blue histograms show the distribution of the contaminants with the old definitions, while the shaded blue histograms show the distribution of the contaminants with the new selection criterion as defined in section 4.5. The upper plot shows the diagram obtained for  $z \leq 0.5$ , and the lower plot shows the diagram obtained for  $z > 0.5$ .

of the criterion adopted. This contamination has been shown to be dependent on the stellar mass for all the samples, with more massive samples being less biased than less massive ones. This fact demonstrates that a cut in stellar mass is helpful to improve the purity of the sample.

- The comparison between the different selection criteria shows that the best performing one is based on a combined selection since it takes into account all the available information about the galaxies (morphological, spectroscopic and photometric), with the obvious disadvantage of being highly demanding in terms of the data needed. For this sample, we find that the contamination is minimized, especially for stellar masses  $\log(\mathcal{M}/M_\odot) > 10.25$ :  $< 10\%$  for both optical and IRAC colors,  $\lesssim 10\%$  in sSFR and with weak emission line equivalent widths for the contaminants ( $\lesssim 10 \text{ \AA}$ ).

- The morphological criterion is the one with the larger contamination, and a high percentage of blue, emission-line, star-forming elliptical galaxies has been found in this sample ( $\sim 12\text{-}65\%$ , depending on the mass range). Among the other selection criteria, we identify the red SED and the quiescent as the best since their slight increase in contamination (about a factor 2) is offset by the fact that they are extremely economical in terms of information required.
- The slope of the number density as a function of redshift at fixed mass for the various samples is similar. We found an increase in number density in the mass range  $10.25 < \log(\mathcal{M}/\mathcal{M}_{\odot}) < 10.75$  from  $z = 0.65$  to  $z = 0.2$  by a factor  $\sim 2\text{-}4$ , in the mass range  $10.75 < \log(\mathcal{M}/\mathcal{M}_{\odot}) < 11$  from  $z = 1$  to  $z = 0.2$  by a factor  $\sim 2\text{-}3$ , while for massive ETGs  $11 < \log(\mathcal{M}/\mathcal{M}_{\odot}) < 11.5$  this increase from  $z = 1$  to  $z = 0.2$  is only  $\sim 10\text{-}50\%$  (and  $< 10\%$  between  $z = 1$  and  $z = 0.4$ ). This trend in mass confirms that most massive ETGs are already in place at  $z \sim 1$ . The comparison of the different number densities suggests a scenario for ETGs in which the color transformation from blue to red precedes the quenching of the star formation and the morphological transformation from late type to ellipticals.
- By analyzing the color-mass and color-color diagrams, we proposed two revised selection criteria, which help to reduce the contamination by blue star-forming galaxies.

Selecting a sample of passive galaxies that is as uncontaminated as possible by star-forming objects is crucial for an unbiased study of the properties of this population of galaxies. The analysis presented in this paper provides a first detailed comparison of the contamination obtained with different selection criteria, and represents an important step forward in the identification of the best ways of selecting passive galaxies. This will be especially fundamental for the new and upcoming surveys such as BOSS (Schlegel et al., 2009) and Euclid (Laureijs et al., 2011), which will provide the scientific community unprecedented statistics of these objects, in particular at high redshift. From this point of view, this work represents the starting point to study and develop optimized passive galaxy selection criteria also at  $z > 1$ , which could be applied, for example, to Euclid simulations.

In a forthcoming paper we aim to study how much the different selections presented here affect the study of the evolution of passive galaxies.

*Acknowledgements.* MM and AC acknowledge the grants ASI n.I/023/12/0 “Attività relative alla fase B2/C per la missione Euclid” and MIUR PRIN 2010-2011 “The dark Universe and the cosmic evolution of baryons: from current surveys to Euclid”. Part of the work has also been supported by an INAF grant “PRIN-2010”. This analysis is based on zCOSMOS observations, carried out using the Very Large Telescope at the ESO Paranal Observatory under Programme ID: LP175.A-0839. We would like to thank the anonymous referee for the useful comments and suggestions, which helped to improve the paper.

## References

Annibali F., Bressan A., Rampazzo R., et al., 2010, *A&A*, 519, A40  
 Aviles A., Bravetti A., Capozziello S., et al., 2013, *PhRvD*, 87, 044012  
 Baldry I. K., Glazebrook K., Brinkmann J., et al., 2004, *ApJ*, 600, 681  
 Baldry I. K., Balogh M. L., Bower R., et al., 2004, *AIPC*, 743, 106

Baldry I. K., Balogh M. L., Bower R. G., et al., 2006, *MNRAS*, 373, 469  
 Baldry I. K., Glazebrook K., Driver S. P., 2008, *MNRAS*, 388, 945  
 Baldwin J. A., Phillips M. M., Terlevich R., 1981, *PASP*, 93, 5  
 Balogh M., Eke V., Miller C., et al., 2004, *MNRAS*, 348, 1355  
 Bell E. F., Wolf C., Meisenheimer K., et al., 2004, *ApJ*, 608, 752  
 Brammer G. B., Whitaker K. E., van Dokkum P. G., et al., 2011, *ApJ*, 739, 24  
 Brinchmann J., Charlot S., White S. D. M., et al., 2004, *MNRAS*, 351, 1151  
 Bruzual G., Charlot S., 2003, *MNRAS*, 344, 1000  
 Bundy K., Ellis R. S., Conselice C. J., et al., 2006, *ApJ*, 651, 120  
 Calzetti D., Armus L., Bohlin R. C., et al., 2000, *ApJ*, 533, 682  
 Capak P., Aussel H., Ajiki M., et al., 2007, *ApJS*, 172, 99  
 Chabrier G., 2003, *PASP*, 115, 763  
 Cimatti A., Daddi E., Renzini A., 2006, *A&A*, 453, L29  
 Coleman G. D., Wu C.-C., Weedman D. W., 1980, *ApJS*, 43, 393  
 Davidson I., Bolzonella M., Coupon J., et al., 2013, arXiv:1303.3808  
 Donley J. L., Scodreggio M., Garilli B., et al., 2012, *ApJ*, 748, 142  
 Drory N., Salvato M., Gabasch A., et al., 2005, *ApJ*, 619, L131  
 Eisenstein D. J., Annis J., Gunn J. E., et al., 2001, *AJ*, 122, 2267  
 Fontana A., Pozzetti L., Donnarumma I., et al., 2004, *A&A*, 424, 23  
 Franzetti P., Scodreggio M., Garilli B., et al., 2007, *A&A*, 465, 711  
 Garilli B., Fumana M., Franzetti P., et al., 2010, *PASP*, 122, 827  
 Heckman T. M., 1980, *A&A*, 87, 152  
 Hogg D. W., Blanton M., Strateva I., et al., 2002, *AJ*, 124, 646  
 Ilbert O., Arnouts S., McCracken H. J., et al., 2006, *A&A*, 457, 841  
 Ilbert O., Capak P., Salvato M., et al., 2009, *ApJ*, 690, 1236  
 Ilbert O., Salvato M., Le Floc’h E., et al., 2010, *ApJ*, 709, 644  
 Ilbert O., McCracken H. J., Le Fèvre O., et al., 2013, arXiv:1301.3157  
 Jimenez R., Loeb A., 2002, *ApJ*, 573, 37  
 Hubble E. P., 1936, Oxford University Press, 45  
 Kauffmann G., Heckman T. M., White S. D. M., et al., 2003, *MNRAS*, 341, 54  
 Kinney A. L., Calzetti D., Bohlin R. C., et al., 1996, *ApJ*, 467, 38  
 Koekemoer A. M., Aussel H., Calzetti D., et al., 2007, *ApJS*, 172, 196  
 Lacy M., Storr-Lombardi L. J., Sajina A., et al., 2004, *ApJS*, 154, 166  
 Lamareille F., Contini T., Le Borgne J.-F., et al., 2006, *A&A*, 448, 893  
 Laureijs R., Amiaux J., Arduini S., et al., 2011, arXiv:1110.3193  
 Le Fèvre O., Saisse M., Mancini D., et al., 2003, *SPIE*, 4841, 1670  
 Le Fèvre O., Vettolani G., Garilli B., et al., 2005, *A&A*, 439, 845  
 Lilly S. J., Le Fèvre O., Renzini A., et al., 2007, *ApJS*, 172, 70  
 Lilly S. J., Le Brun V., Maier C., et al., 2009, *ApJS*, 184, 218  
 Maraston C., Pforr J., Henriques B. M., et al., 2012, arXiv:1207.6114  
 Masters K. L., Maraston C., Nichol R. C., et al., 2011, *MNRAS*, 418, 1055  
 Meneux B., Le Fèvre O., Guzzo L., et al., 2006, *A&A*, 452, 387  
 Mignoli M., Zamorani G., Scodreggio M., et al., 2009, *A&A*, 493, 39  
 Moresco M., Pozzetti L., Cimatti A., et al., 2010, *A&A*, 524, A67  
 Moresco M., Jimenez R., Cimatti A., et al., 2011, *JCAP*, 3, 45  
 Moresco M., Cimatti A., Jimenez R., et al., 2012, *JCAP*, 8, 6  
 Moresco M., Verde L., Pozzetti L., et al., 2012, *JCAP*, 7, 53  
 Moustakas J., Coil A., Aird J., et al., 2013, arXiv:1301.1688  
 Peng Y.-j., Lilly S. J., Kováč K., et al., 2010, *ApJ*, 721, 193  
 Phillips M. M., Jenkins C. R., Dopita M. A., et al., 1986, *AJ*, 91, 1062  
 Polletta M., Tajer M., Maraschi L., et al., 2007, *ApJ*, 663, 81  
 Pozzetti L., Bolzonella M., Zucca E., et al., 2010, *A&A*, 523, A13  
 Renzini A., 2006, *ARA&A*, 44, 141  
 Riemer-Sørensen S., Parkinson D., Davis T. M., et al., 2013, *ApJ*, 763, 89  
 Said N., Baccigalupi C., Martinelli M., et al., 2013, arXiv:1303.4353  
 Scarlata C., Carollo C. M., Lilly S. J., et al., 2007, *ApJS*, 172, 406  
 Scarlata C., Carollo C. M., Lilly S. J., et al., 2007, *ApJS*, 172, 494  
 Schlegel D., White M., Eisenstein D., 2009, in *Astronomy*, Vol. 2010, astro2010: The Astronomy and Astrophysics Decadal Survey, p. 314  
 Schmidt M., 1968, *ApJ*, 151, 393  
 Scodreggio M., Franzetti P., Garilli B., et al., 2005, *PASP*, 117, 1284  
 Scoville N., Aussel H., Brusa M., et al., 2007, *ApJS*, 172, 1  
 Simon J., Verde L., Jimenez R., 2005, *PhRvD*, 71, 123001  
 Stern D., Jimenez R., Verde L., et al., 2010, *JCAP*, 2, 8  
 Strateva I., Ivezić Ž., Knapp G. R., et al., 2001, *AJ*, 122, 1861  
 Silva L., Granato G. L., Bressan A., et al., 1998, *ApJ*, 509, 103  
 Thomas D., Maraston C., Schawinski K., et al., 2010, *MNRAS*, 404, 1775  
 Tully R. B., Mould J. R., Aaronson M., 1982, *ApJ*, 257, 527

- Tasca L. A. M., Kneib J.-P., Iovino A., et al., 2009, *A&A*, 503, 379  
 Visvanathan N., Sandage A., 1977, *ApJ*, 216, 214  
 Wang X., Meng X.-L., Zhang T.-J., et al., 2012, *JCAP*, 11, 18  
 Williams R. J., Quadri R. F., Franx M., et al., 2009, *ApJ*, 691, 1879  
 Yan R., Newman J. A., Faber S. M., et al., 2006, *ApJ*, 648, 281  
 Yan R., Blanton M. R., 2012, *ApJ*, 747, 61  
 Zehavi I., Zheng Z., Weinberg D. H., et al., 2011, *ApJ*, 736, 59  
 Zucca E., Ilbert O., Bardelli S., et al., 2006, *A&A*, 455, 879  
 Zucca E., Bardelli S., Bolzonella M., et al., 2009, *A&A*, 508, 1217
- 

<sup>1</sup> Dipartimento di Fisica e Astronomia, Università degli Studi di Bologna, V.le Bertini Pichat, 6/2 - 40127, Bologna, Italy

<sup>2</sup> INAF – Osservatorio Astronomico di Bologna, via Ranzani 1, I-40127, Bologna, Italy

<sup>3</sup> Institut de Recherche en Astrophysique et Planétologie, CNRS, F-31400 Toulouse, France

<sup>4</sup> Institute for Astronomy, ETH Zurich, 8093 Zurich, Switzerland

<sup>5</sup> IRAP, Université de Toulouse, UPS-OMP, Toulouse, France

<sup>6</sup> Laboratoire d’Astrophysique de Marseille, Aix Marseille Université, CNRS, 13388, Marseille, France

<sup>7</sup> European Southern Observatory, Garching, Germany

<sup>8</sup> INAF – Osservatorio Astronomico di Padova, Padova, Italy

<sup>9</sup> INAF – Istituto di Astrofisica Spaziale e Fisica Cosmica, Milano, Italy

<sup>10</sup> INAF – Osservatorio Astronomico di Roma, 00040, Monteporzio Catone, Italy

<sup>11</sup> Institute for Astronomy, The University of Edinburgh, Royal Observatory, Edinburgh, EH93HJ, UK

<sup>12</sup> INAF – Osservatorio Astronomico di Brera, Milano, Italy

<sup>13</sup> Space Telescope Science Institute, Baltimore, MD 21218, USA

<sup>14</sup> Kavli Institute for the Physics and Mathematics of the Universe (WPI), Todai Institutes for Advanced Study, The University of Tokyo, 5-1-5 Kashiwanoha, Kashiwa, 277-8583, Japan

<sup>15</sup> INAF – Istituto di Astrofisica Spaziale e Fisica Cosmica, Bologna, Italy

<sup>16</sup> Institute for Astronomy, University of Hawaii, 2680 Woodlawn Drive, Honolulu, HI 96822, USA

<sup>17</sup> Institut d’Astrophysique de Paris, Université Pierre & Marie Curie, 75014 Paris, France

<sup>18</sup> UC Santa Cruz/UCO Lick Observatory, 1156 High Street, Santa Cruz, CA 95064, USA

<sup>19</sup> Minnesota Institute for Astrophysics, School of Physics and Astronomy, University of Minnesota, Minneapolis, MN 55455, USA

<sup>20</sup> California Institute of Technology, MC 249-17, 1200 East California Boulevard, Pasadena, CA 91125, USA

<sup>21</sup> Institut d’Astrophysique Spatiale, Batiment 121, CNRS & Univ. Paris Sud XI, 91405 Orsay Cedex, France

<sup>22</sup> Centro de Estudios de Física del Cosmos de Aragón, Plaza San Juan 1, planta 2, 44001, Teruel, Spain

<sup>23</sup> Kapteyn Astronomical Institute, University of Groningen, P.O. Box 800, 9700 AV Groningen, The Netherlands

<sup>24</sup> University of Vienna, Department of Astrophysics, Tuerkenschanzstrasse 17, 1180 Vienna, Austria